

1 **Faster processing of moving compared to flashed bars in awake macaque V1 provides a neural**  
2 **correlate of the flash lag illusion**

3

4 ***Abbreviated title: Neural correlates of flash lag illusion***

5 Manivannan Subramaniyan<sup>1,+</sup>, Alexander S. Ecker<sup>1,2,3,7</sup>, Saumil S. Patel<sup>1</sup>, R. James Cotton<sup>1</sup>, Matthias  
6 Bethge<sup>2,3,4,7</sup>, Xaq Pitkow<sup>1,7,8</sup>, Philipp Berens<sup>1,2,3,5</sup> and Andreas S. Tolias<sup>1,3,6,7,\*</sup>

7

8

9

10  
11 <sup>1</sup>Department of Neuroscience, Baylor College of Medicine, Houston, Texas 77030, USA.

12 <sup>2</sup>Werner Reichardt Centre for Integrative Neuroscience, University of Tübingen, 72076 Tübingen, Germany.

13 <sup>3</sup>Bernstein Center for Computational Neuroscience Tübingen, 72076 Tübingen, Germany.

14

15 <sup>4</sup>Max Planck Institute for Biological Cybernetics, 72076 Tübingen, Germany.

16

17 <sup>5</sup>Institute for Ophthalmic Research, University of Tübingen, 72076 Tübingen, Germany.

18

19 <sup>7</sup>Center for Neuroscience and Artificial Intelligence, Baylor College of Medicine, Houston, TX, 77030, USA.

20

21 <sup>8</sup>Department of Electrical and Computer Engineering, Rice University, Houston, Texas 77005, USA.

22

23 <sup>+</sup>Department of Neuroscience, Perelman School of Medicine, University of Pennsylvania, Philadelphia, 19104,  
24 USA.

25

26

27 *Corresponding author:*

28 Andreas S. Tolias

29 Department of Neuroscience

30 Baylor College of Medicine

31 Houston, Texas 77030, USA

32 Email: [astolias@bcm.edu](mailto:astolias@bcm.edu)

33 Phone: 713-798-4071

34

35

36

37

38

39

40

41

42

43

44 **Abstract**

45 When the brain has determined the position of a moving object, due to anatomical and processing delays, the  
46 object will have already moved to a new location. Given the statistical regularities present in natural motion, the  
47 brain may have acquired compensatory mechanisms to minimize the mismatch between the perceived and the  
48 real position of a moving object. A well-known visual illusion — the flash lag effect — points towards such a  
49 possibility. Although many psychophysical models have been suggested to explain this illusion, their  
50 predictions have not been tested at the neural level, particularly in a species of animal known to perceive the  
51 illusion. Towards this, we recorded neural responses to flashed and moving bars from primary visual cortex  
52 (V1) of awake, fixating macaque monkeys. We found that the response latency to moving bars of varying  
53 speed, motion direction and luminance was shorter than that to flashes, in a manner that is consistent with  
54 psychophysical results. At the level of V1, our results support the differential latency model positing that  
55 flashed and moving bars have different latencies. As we found a neural correlate of the illusion in passively  
56 fixating monkeys, our results also suggest that judging the instantaneous position of the moving bar at the time  
57 of flash — as required by the postdiction/motion-biasing model — may not be necessary for observing a neural  
58 correlate of the illusion. Our results also suggest that the brain may have evolved mechanisms to process  
59 moving stimuli faster and closer to real time compared with briefly appearing stationary stimuli.

60 **New and Noteworthy**

61 We report several observations in awake macaque V1 that provide support for the differential latency model of  
62 the flash lag illusion. We find that the equal latency of flash and moving stimuli as assumed by motion  
63 integration/postdiction models does not hold in V1. We show that in macaque V1, motion processing latency  
64 depends on stimulus luminance, speed and motion direction in a manner consistent with several psychophysical  
65 properties of the flash lag illusion.

66 **Key words:** Flash lag illusion, V1, monkey, latency, motion

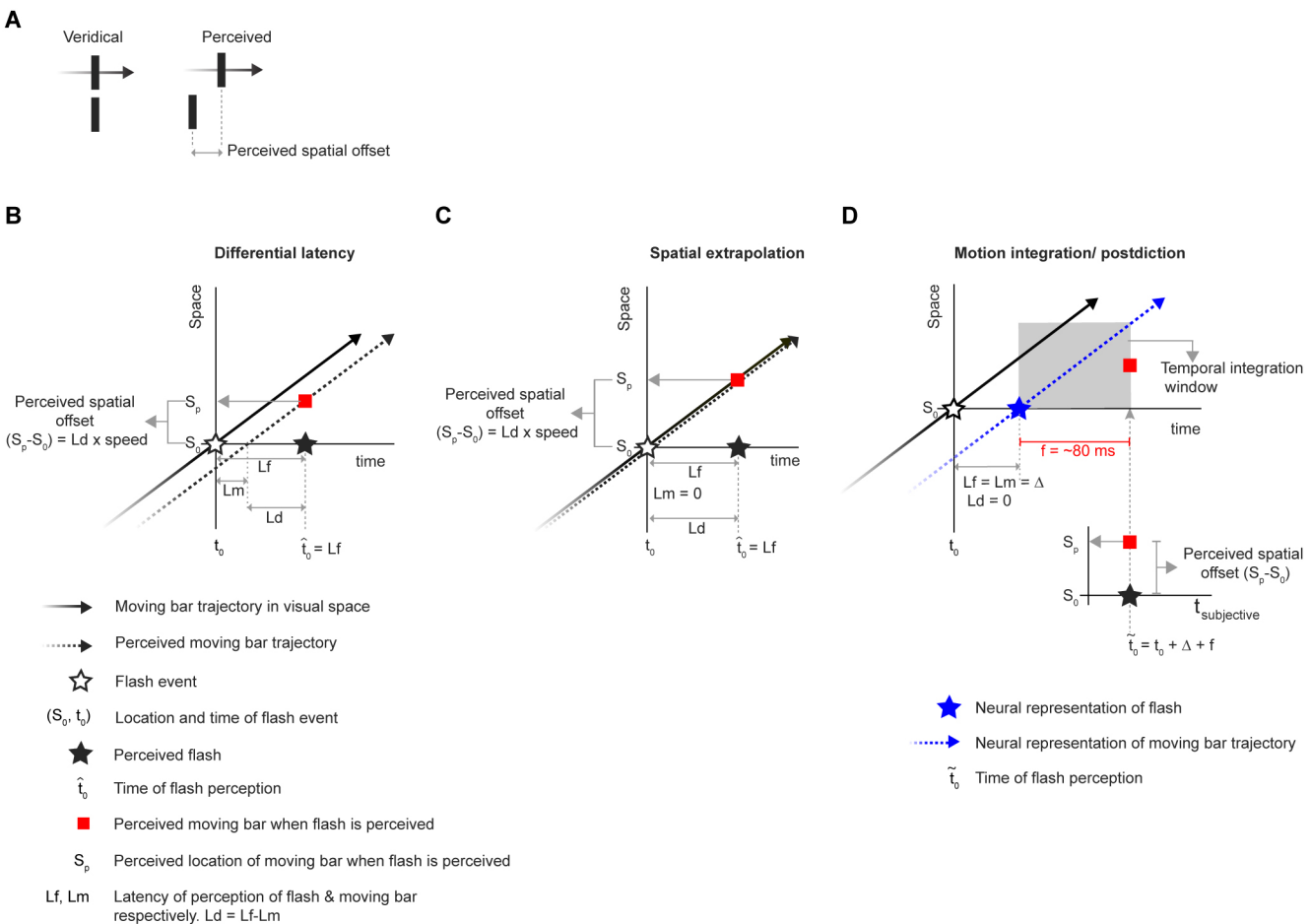
67 **Introduction**

68 Moving objects in nature typically follow smooth, predictable trajectories, potentially enabling the brain to  
69 minimize or compensate for motion processing delays. The flash lag illusion has kindled much interest among  
70 neuroscientists as it is thought to provide a window into the neural mechanisms of localizing moving objects. In  
71 this illusion, observers report that a moving bar is located ahead of an aligned flash (**Fig. 1A**) (Mackay 1958;  
72 Nijhawan 1994). While this phenomenon has been studied extensively at the behavioral level, its underlying  
73 neural mechanisms are poorly understood.

74 In an initial attempt to explain this illusion, it was posited that the brain extrapolates the position of moving  
75 stimuli to an extent that compensates its own processing delays (Nijhawan 1994). Since then, many alternative  
76 models have been proposed. These diverse models (**Fig. 1B-D**), reviewed extensively elsewhere (Eagleman and  
77 Sejnowski 2007; Öğmen et al. 2004), have pointed towards equally diverse neural mechanisms which range  
78 from simple bottom-up explanations such as latency differences to high level top-down mechanisms such as  
79 attention and feedback (Bachmann and Poder 2001; Baldo and Klein 1995; Brenner and Smeets 2000;  
80 Eagleman and Sejnowski 2007; Krekelberg and Lappe 2000; Patel 2000; Purushothaman et al. 1998; Sheth et  
81 al. 2000; Whitney and Murakami 1998). For example, the differential latency model (Purushothaman et al.  
82 1998; Whitney and Murakami 1998) maintains that moving stimuli are processed faster compared to flashed  
83 ones, leading to the perception of flashes temporally coinciding with a moving bar further along its trajectory.  
84 Alternatively, the motion-biasing model (Eagleman and Sejnowski 2007; Rao et al. 2001) argues that motion  
85 signals after the detection of flash event affect position representation and judgments, such that observers report  
86 a misalignment between a flash and a moving stimulus. There has also been a recent attempt to subsume all  
87 these models into a single theoretical framework treating the flash lag effect as a probabilistic motion-based  
88 predictive shift (Khoei et al. 2017).

89 Most models of the flash lag illusion are formulated at the psychophysical level. At this level of abstraction, the  
 90 three most prominent models (**Fig. 1B-D**) of the illusion differ in their prediction for the relative latencies of  
 91 flashed and moving stimuli (**Fig. 2**). In this context, the latency or "representation delay" refers to the time  
 92 interval between stimulus appearance at a particular location in the physical world and the emergence of neural  
 93 activity corresponding to the reported perception of the stimulus location. The spatial extrapolation model, as it  
 94 posits full compensation for neural delays (Nijhawan 1994), would predict zero representation delay for motion;  
 95 the differential latency model predicts shorter latency for motion (Patel 2000; Purushothaman et al. 1998;  
 96 Whitney and Murakami 1998) and the postdiction model assumes equal latency for flash and moving stimuli  
 97 (Eagleman and Sejnowski 2007; Rao et al. 2001). The models do not specify in which part of the brain one  
 98 would observe such predicted latency differences of stimulus representations. Here, to systematically  
 99 investigate the neural mechanisms of the flash lag illusion and to test predictions of the psychophysical models,  
 100 we measured the latencies or representation delays of flashed and moving stimuli in primary visual cortex (V1)  
 101 of awake, fixating macaques. This allows us to determine the contribution of early visual processing towards the  
 102 illusion. Note that, at the level of V1, the term latency or "representation delay" refers to the time interval  
 103 between stimulus appearance at a particular location in the physical world and the time of stimulus-evoked  
 104 activity in V1 at which a decoder or a downstream processing region can obtain the best estimate of the  
 105 stimulus location (see Methods).

106



107

108 **Fig. 1.** Models of flash lag illusion. **A**, When a flash (bottom) is presented aligned to a moving bar (top), observers  
 109 perceive the moving bar to be located further along the motion trajectory at the moment when they perceive the flash. Left:

110 veridical locations; right: perceived locations. Since the flash appears to spatially lag behind the moving bar, this  
111 phenomenon has been called the flash lag illusion. In all panels (**A-D**), motion is assumed to have started long before the  
112 flash event. **B-D**, Illustration of flash lag effect as explained by different models. **B**, Differential latency model. The flash  
113 (open star) presented at time  $t_0$  at location  $S_0$  is perceived with a latency of  $L_f$ . Since the model assumes a shorter motion  
114 latency ( $L_m < L_f$ ), when the flash is perceived (filled star), the moving bar located (at  $S_p$ , red square) further along the  
115 trajectory is perceived to be aligned with flash. **C**, In the spatial extrapolation model, the moving bar is perceived ahead of  
116 the flash due to the longer latency of flash like in **B** except that the motion latency is assumed to be zero. **D**, Illustration of  
117 the postdiction model, adapted from Fig. 2 of Rao et al (2001). In this model, the nervous system completes processing the  
118 flash at  $t_0+\Delta$  at which point the motion integration that lasts for a duration of  $f$  is triggered. Although in the other models  
119 the flash is perceived at  $t_0+\Delta$ , postdiction model claims that the perception of the flash is delayed until  $t_0+\Delta+f$  at which  
120 point the motion integration based moving bar position estimation is completed (Rao et al. 2001). Hence, although in the  
121 external time, motion integration based moving bar position is obtained at time  $t_0+\Delta+f$  and flash representation is  
122 completed earlier at  $t_0+\Delta$ , in the subjective time, they are perceived simultaneous, giving raise to the perceived spatial  
123 offset.

124 The few physiological studies that have explored the neural mechanisms of the illusion found a shorter latency  
125 for motion signals compared to flashes in the rabbit and salamander retina (Berry et al. 1999), cat LGN (Orban  
126 et al. 1985) and cat V1 (Jancke et al. 2004b), providing evidence for a bottom up latency difference between  
127 flashes and moving stimuli. Although these studies provide valuable hints at plausible neural mechanisms of the  
128 flash lag illusion, they were done either *in vitro* or in anesthetized animals and it is unknown if the animals used  
129 in these studies actually perceive the illusion.

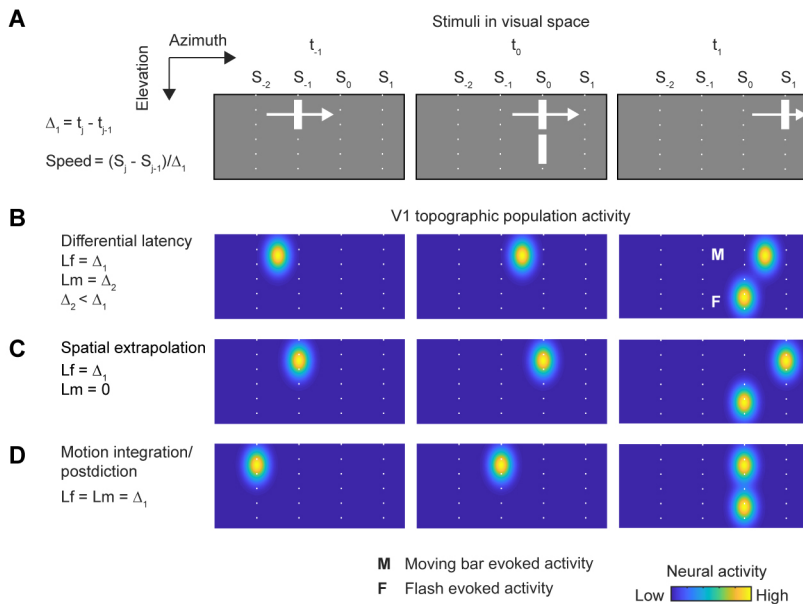
130 We previously showed that, similar to humans, macaque monkeys perceive the flash lag illusion (Subramaniyan  
131 et al. 2013). Hence, we performed the physiological experiments in awake macaque monkeys, which allowed us  
132 to directly test the predictions of different models of the illusion at the level of V1 neural representation of flash  
133 and moving stimuli (**Fig. 2**). Specifically, we estimated the latency of the stimulus representations by two  
134 different methods, one based on multiunit response peak times and the other based on probabilistic decoding of  
135 simultaneously recorded single- and multiunit population activity. Crucially, we measured the dependence of  
136 latency on different stimulus parameters — speed, luminance and direction of motion — to test if the resulting  
137 changes in neural responses accounted for the corresponding changes in perception. Under all these  
138 manipulations, neural latency differences between flash and motion in V1 explained a large part of the  
139 psychophysically measured perceived spatial offsets. Thus, our results show that even at the very first cortical  
140 visual information processing stage a neural correlate of the illusion can be observed, providing mechanistic  
141 constraints on the models of the flash lag illusion.

## 142 Materials and Methods

143 **Subjects.** Four male macaque (*Macaca mulatta*) monkeys (A, CH, CL and L) weighing 8, 9, 12 and 9.5 kg  
144 respectively and aged 10, 8, 8 and 8 years respectively, were used in the physiological experiments. Cranial  
145 head post and scleral search coil were implanted in each monkey using standard aseptic surgical procedures. All  
146 animal procedures were approved by the Institutional Animal Care and Use Committee of Baylor College of  
147 Medicine and followed NIH regulations. Two of the authors (MS and SP) participated in psychophysical  
148 experiments following procedures approved by the Institutional Review Board of Baylor College of Medicine.

149 **Electrophysiological recording and data processing.** We used chronically implanted tetrode arrays for  
150 recording neural activity from monkeys A, CL and CH as described previously (Ecker et al. 2010; Tolias et al.  
151 2007). Briefly, in each monkey, we implanted chronically, arrays of 24 tetrodes on the left hemisphere over the  
152 operculum in area V1. The tetrodes were custom built from Nichrome or Platinum/Iridium wires. We implanted  
153 a 96-electrode microelectrode array ('Utah' array, Blackrock Microsystems, Salt Lake City, UT, USA) over  
154 area V1 on the right hemisphere in monkey L. For both tetrode arrays and Utah array, the neural signals were  
155 pre-amplified at the head-stage by unity gain preamplifiers (HS-27, Neuralynx, Bozeman MT, USA). These  
156 signals were then digitized with 24-bit analog data acquisition cards with 30 dB onboard gain (PXI-4498,  
157 National Instruments, Austin, TX) and sampled at 32 kHz. Broadband signals (0.5 Hz – 16 kHz) were

158 continuously recorded using custom-built LabVIEW software for the duration of the experiment. For tetrode  
 159 array data, the spike detection and spike sorting methods have been described previously (Ecker et al. 2014;  
 160 Tolias et al. 2007). For the Utah array, spikes were detected from individual electrodes following the same  
 161 procedure. In this study, the term ‘multiunit’ refers to the set of all the spikes detected from a single tetrode or a  
 162 single electrode (Utah array).



163

164 **Fig. 2.** Predictions of models of flash lag illusion for V1 population activity for continuous motion condition with identical  
 165 flash and moving bar luminance. In all panels (**A-D**), motion is assumed to have started long before the flash event. **A**,  
 166 Illustration of hypothetical visual stimuli that generate the population activity in V1 as predicted by different models (**B-D**).  
 167 For simplicity, the stimulus positions are shown at just three time instances  $t_1$ ,  $t_0$  and  $t_1$ . The time the moving bar takes ( $\Delta_1$   
 168 =  $t_j - t_{j-1}$  ms) to traverse from  $S_j$  to  $S_{j-1}$  is also set to be equal to the latency of population activity peak for flash (**B-D**). **B-D**,  
 169 Illustrations showing predicted topographically organized V1 population neural response to stimuli depicted in matching  
 170 panels in **A**. The flash is assumed to be fully represented in V1 when the population hill reaches its peak activity at  $S_0$ . In  
 171 the moving bar condition, a fully developed population activity hill (white label ‘M’) representing some position,  
 172 continuously translates following the motion trajectory. Hence which position of moving bar caused an activity hill at a  
 173 given instant will depend on the motion population response peak latency. For all models, the neural representation of flash  
 174 (white label ‘F’) in V1 is delayed by the same duration  $\Delta_1$ . The models differ in the neural representation delays of moving  
 175 bar as seen at time instant  $t_1$ : the differential latency model (**B**) predicts that the population hill will spatially lag behind the  
 176 moving bar but will be shifted along the motion direction relative to flash population hill. The spatial extrapolation model  
 177 (**C**) predicts a similar shift of the motion population hill relative to flash. However, the motion population hill does not  
 178 spatially lag behind the moving bar. The postdiction model (**D**) assumes identical latency for flash and moving bar neural  
 179 representations - hence the population hills will be aligned.

180

181 **Behavioral task.** Visual stimuli were presented in a dark room using dedicated graphics workstations using  
 182 Psychophysics Toolbox 3 (Brainard 1997; Kleiner 2007; Pelli 1997). For all experiments with monkeys A, CH  
 183 and CL we presented stimuli on CRT monitors (model: Sgi C220 Flat Diamondtron; display size:  $22 \times 16^\circ$  from  
 184 a distance of 100 cm; resolution:  $1600 \times 1200$  pixels; refresh rate: 100 Hz). For monkey L, we presented stimuli  
 185 on an LCD monitor (Samsung – model S23A950D; refresh rate of 120 Hz; monitor resolution:  $1920 \times 1080$   
 186 pixels, subtending visual angles of  $29 \times 16^\circ$  from a viewing distance of 100 cm). We gamma-corrected the  
 187 monitors to achieve a linear luminance response profile. The monitor background luminance was  $6.1 \text{ cd/m}^2$   
 188 (monkeys CL & A),  $9.5 \text{ cd/m}^2$  (monkey CH) or  $0.04 \text{ cd/m}^2$  (monkey L). The monkeys sat in a custom primate

189 chair at 100 or 107 cm from the stimulus display monitor. Eye positions were continuously monitored online  
190 with scleral search coil for monkeys A, CH and CL and using a custom-built video tracker (frame rate: 250Hz)  
191 for monkey L. Eye position signals were also saved for offline analysis. Each trial (**Fig. 4A**) began with a brief  
192 sound that instructed the monkeys to start fixating at a red dot (0.12– 0.14°) within a circular window of radius  
193 of 0.5–0.6° of visual angle. After the monkeys fixated for 300 ms, we presented different visual stimuli. The  
194 monkeys fixated for an additional 300 ms after the stimulus offset. For successfully completing the trials, the  
195 monkeys received juice or water reward. The next trial began after an inter-trial time of 1500 ms.

196 *Receptive field mapping.* We mapped the spatiotemporal receptive fields using a white noise random dot  
197 stimulus. On a gray background, we presented black and white squares (0.11–0.14° side) on a rectangular grid  
198 covering the receptive field of all recorded neurons. The squares were presented one at a time for three video  
199 frames (25–30 ms) in a pseudorandom sequence for 1200–2000 ms. The sequence consisted of many iterations,  
200 in each of which every grid location was visited exactly once in a random order, thus balancing the number of  
201 times each location was visited over the course of the experiment. The monkeys performed  $242 \pm 56$  trials  
202 (mean  $\pm$  S.D.) in a session that lasted for around 20 min. Since primate V1 contains many complex cells and we  
203 were interested primarily in the location of the receptive fields, we performed reverse correlation ignoring the  
204 sign of the stimulus (i.e. both black and white were treated as positive). We assessed the quality of the receptive  
205 field estimation by the following heuristic method. We first averaged the receptive field maps obtained at lags  
206 ranging from 40 to 100 ms, resulting in a single spatial kernel for each multiunit. We fitted the spatial kernel  
207 with a two-dimensional Gaussian and computed the percentage of variance explained (across pixels) by the  
208 model. For all analyses in this study, we included multiunits for which the model explained more than 75% of  
209 the variance. From the model fitting, we also extracted receptive field centers and outlines. For illustration we  
210 outlined receptive fields by the elliptical contour at two standard deviations from the center.

211 *Speed manipulation experiment.* Monkeys A, CH and CL were used in this experiment. Moving and flashed  
212 vertical bars of identical luminance and size ( $0.28 \times 1.7^\circ$ ) were used as visual stimuli. The bar luminance was  
213 either 23 cd/m<sup>2</sup> (monkeys A & CL) or 37 cd/m<sup>2</sup> (monkey CH). We defined a stimulus presentation center for  
214 each monkey as the average of the receptive field centers (ARFC) of the neurons we recorded from; the mean  
215 eccentricity of this location was  $1.5 \pm 0.11^\circ$  (azimuth:  $0.87 \pm 0.3^\circ$  and elevation:  $1.2 \pm 0.3^\circ$ ; mean  $\pm$  S.D.). In  
216 each stimulus period, only a flash or a moving bar was presented. We presented flashes for one video frame (10  
217 ms). Since we recorded from many neurons simultaneously, to stimulate all the recorded neurons, we presented  
218 flashes at 5–7 locations around the ARFC (**Fig. 4B**). These locations were abutting each other without any  
219 overlap. The trajectory length of the moving bar was 4.6 or 5.4°. The midpoint of the moving bar's trajectory  
220 was at the ARFC. The moving bar translated horizontally from left to right or from right to left at one of three  
221 speeds: 7, 14 or 28°/s (range: 6.9–7.4, 13.8–14.7 and 27.5–29.5 °/s respectively). All stimulus conditions were  
222 presented with equal probability. In each trial (**Fig. 4A**), we chose more than one stimulus condition randomly  
223 (two flashes and one moving stimulus for example) and presented them one after the other with an inter-  
224 stimulus period of 300 ms; this allowed us to use the monkeys' fixating period efficiently and present multiple  
225 stimulus conditions within every trial. During the stimulus period of  $\leq 1800$  ms, we presented  $4 \pm 1$  (mean  $\pm$   
226 S.D.) stimuli. In a session, we repeated each stimulus condition for  $426 \pm 216$  (mean  $\pm$  S.D.) times. The  
227 monkeys performed  $1597 \pm 718$  (mean  $\pm$  S.D.) trials per session. Each session lasted for  $3 \pm 1$  (mean  $\pm$  S.D.)  
228 hours.

229 *Luminance manipulation experiment.* Monkey L was used in this experiment. The stimulus presentation  
230 followed the same overall design as the speed manipulation experiment (see above) with the following  
231 exceptions. The size of the bar was  $0.15 \times 1.8^\circ$ . Moving and flashed bars with luminance values of 0.24, 0.82,  
232 9.4, 48 cd/m<sup>2</sup> were presented in each session. Flashes were presented at one of nine abutting locations with the  
233 ARFC at an eccentricity of  $0.92 \pm 0.07^\circ$  (azimuth  $-0.46 \pm 0^\circ$  and elevation  $0.79 \pm 0.08^\circ$ ; mean  $\pm$  S.D.). The  
234 trajectory length of the moving bar was 8.7°. The moving bar translated horizontally from left to right or from  
235 right to left at 18°/s. In the stimulus period of each trial, we presented  $5 \pm 1$  (mean  $\pm$  S.D.) stimuli. Each  
236 stimulus condition was repeated  $120 \pm 46$  (mean  $\pm$  S.D.) times. The monkey performed  $1128 \pm 432$  (mean  $\pm$

237 S.D.) trials per session with each session lasting  $2 \pm 1$  (mean  $\pm$  S.D.) hours. Note that to fit all luminance  
238 conditions within the recording duration, we did not test multiple speeds. Instead we chose a speed ( $18^\circ/\text{s}$ ) that  
239 was intermediate between speeds  $7$  and  $28^\circ/\text{s}$  that were used in the speed manipulation experiment. We also  
240 reduced the width of the bar to roughly half ( $0.15^\circ$ ) that of the bar used in the speed manipulation experiment  
241 ( $0.28^\circ$ ) so that when the bar moves, the footprints of the bars in the trajectory are contiguous without overlap or  
242 leaving a gap between adjacent instantaneous positions. The flash duration (8.3 ms) is also shorter than that  
243 used for speed manipulation (10ms) because we had to use an LCD monitor which had a higher refresh rate  
244 (120 Hz). We specifically chose an LCD monitor over the CRT monitor because to test very low luminance  
245 levels, we had to set the background luminance to lowest possible value; at that setting (but not at the  
246 background used in speed manipulation experiment), when the bar moved on the CRT monitor, it left behind a  
247 trail of phosphorescence that was obvious to a human observer. Such trailing luminance was not observed on  
248 the LCD monitor.

249 *Control experiment.* Monkeys A and CL were used in this experiment. Stimuli were presented as outlined in the  
250 speed manipulation experiment. However, in addition to presenting flashed and moving bars separately as  
251 above, we also interleaved additional stimulus conditions where we presented the flash and moving bar together  
252 in two arrangements A1 and A2 (**Fig.11A**). In A1, we presented a flash inside the receptive fields and the  
253 moving bar below the flash but outside the receptive fields. To mimic the psychophysical experiment of the  
254 flash lag illusion, in arrangement A1, when the instantaneous position of the moving bar hit the azimuth of the  
255 ARFC, a flash was presented at one of  $5\text{--}7$  horizontal spatial offsets ( $0^\circ, \pm 0.27^\circ, \pm 0.55^\circ, \pm 0.82^\circ$ ). We assigned a  
256 negative sign to the offsets if the flash appeared ahead of the moving bar along the motion direction and a  
257 positive sign if the flash appeared behind the moving bar. In arrangement A2, the vertical positions of the flash  
258 and moving bar in arrangement A1 were interchanged. The moving bar translated at a speed of  $14^\circ/\text{s}$ . The  
259 vertical center-to-center distance between the flash and the moving bar was  $2.1^\circ$ . With the bar height being  $1.7^\circ$ ,  
260 the edge-to-edge gap between the flash and the moving bar was  $0.4^\circ$ . In each trial, we presented  $3\pm 1$  (mean  $\pm$   
261 S.D.) stimulus conditions. Each stimulus condition was repeated  $159\pm 81$  (mean  $\pm$  S.D.) times. The monkeys  
262 completed  $1930\pm 742$  (mean  $\pm$  S.D.) trials per session with each session lasting  $3\pm 1$  (mean  $\pm$  S.D.) hours.

263 *Electrophysiological dataset.* For the entire study, we recorded neural data from a total of 1457 multiunits  
264 (monkey A: 288 CH: 191, CL: 306 and L: 672) over 62 sessions (A: 12, CH: 23, CL: 20 and L: 7) in an average  
265 period of six weeks from each monkey (A: 4, CH: 12, CL: 6 and L: 2). For the flash, relative to the pre-stimulus  
266 fixation period, majority (1038 (71%), A: 247, CH: 180, CL: 276 and L: 335) of the multiunits showed  
267 significantly enhanced responses measured over a window of 30–130 ms after the flash onset. A minority  
268 (44(3%), A: 2, CH: 11, CL: 20 and L: 11) of the multiunits showed flash-evoked suppression. For analyses, we  
269 included a subset of the multiunits (915 (63%), A: 237, CH: 166, CL: 256 and L: 256) that showed enhanced  
270 flash-evoked responses and passed the receptive-field-based selection criterion (955 (66%), A: 247, CH: 176,  
271 CL: 271 and L: 261, see *Receptive field mapping* section). After the above selections, one multiunit from  
272 monkey A was excluded from the analyses in **Fig. 7** and **Fig. 10** as its receptive field center was outside the  
273 flashed region. For the speed manipulation experiment, a total of 163 (A: 57, CH: 56 and CL: 50) single units  
274 were isolated out of which 44% (total: 71, A: 32, CH: 12 and CL: 27) met the selection criteria described above.  
275 For population decoding we chose all the single units from monkey CL since it had the most well-isolated units  
276 (median contamination measure (Tolias et al. 2007)(Interquartile range): CL: 0.039 (0.005, 0.086), CH: 0.076  
277 (0.048, 0.117) and A: 0.092 (0.015, 0.142)).

278 *Response peak delay as neural representation delays for flash and moving stimuli.* For the moving stimuli,  
279 assuming a receptive-field-based labeled-line code for position in V1, the latency of peak activity of a neuron  
280 closely approximates the representation delay. This is because, whenever there is a bar moving in the visual  
281 field, a population activity hill representing some moving bar position is simultaneously present in V1 (**Fig. 2**),  
282 except during the motion onset and offset. We assume that any subsequent visual area decoding moving bar  
283 position based on V1 activity would assign the instantaneous position of the bar center to the position encoded  
284 by the neurons whose activities maximally contribute to the peak of the hill. This would imply that the time at

285 which a given neuron fires maximally is also the time at which the moving population hill activity is centered  
286 over this neuron's topographic location in V1. Under this reasoning, the response peak latency would  
287 correspond to the latency of the V1 representation of the moving bar's instantaneous position. For the flash, the  
288 situation is different because when a flash is presented in the visual field, a population activity hill starts to  
289 develop only after a delay. The hill then rises and falls over time without any change in the position of the peak  
290 of the hill. It is currently unknown at what point in time the activity hill fully represents the flash location. To be  
291 consistent with the method of latency computation of motion, we chose to compute peak response latency for  
292 flash as well.

293 *Estimation of flash response peak latency.* For each flash condition, we first aligned the spike times of a given  
294 stimulus presentation to the flash onset time. We then computed mean firing rates across all stimulus  
295 presentations of a given condition after binning the spikes at half the monitor refresh period (4.2 or 5 ms). In  
296 each session, multiple flashes were presented, covering the receptive field of a given multiunit. We sought to  
297 find the mean firing rate response profile to a flash that was horizontally aligned with the center of the receptive  
298 field. However, there might not be any flash that was presented perfectly over the receptive field center since  
299 we did not optimize the flash locations for any particular neuron. In such cases, the mean firing rate profile that  
300 corresponds to a flash at the receptive field center was obtained by linearly interpolating the mean firing rate  
301 profiles of the flash locations left and right of the receptive field center. The mean firing rate response starting  
302 150 ms before and ending 300 ms after the flash onset was then normalized (z-scored) to have zero mean and  
303 unit variance. After z-scoring, the responses of all multiunits under a given condition were averaged and  
304 smoothed using a Gaussian kernel with a standard deviation of 10 ms. Peak responses latencies were then  
305 computed from these averages. The responses of individual single and multiunits to flashed and moving bars  
306 were sometimes multimodal. Since we had a much larger multiunit dataset compared to single units, we chose  
307 to extract the latencies from responses averaged across multiunits. This procedure turned out to be more robust  
308 than extracting latency for each unit (for a description of how we estimated confidence intervals on the  
309 latencies, see section *Statistical Analysis* below).

310 *Estimation of motion response peak latency.* For each motion condition, we aligned the spike times of a given  
311 presentation to the time at which the moving bar hit the center of the receptive field (i.e., the response time is set  
312 to zero when the moving bar's instantaneous position matched the receptive field center). Since the moving bar  
313 occupied discrete positions along the trajectory that did not necessarily coincide with the receptive field center,  
314 we linearly interpolated the trajectory time points to obtain the time at which the trajectory crossed the receptive  
315 field center. We then computed mean firing rate across all presentations of a given condition after binning the  
316 spikes at half the monitor refresh period (4.2 or 5 ms). The mean firing rate response starting 150 ms before and  
317 ending 300 ms after the zero-time point was then normalized (z-scored) to have zero mean and unit variance.  
318 This normalized response was then averaged across multiunits. After this step, we followed the same procedure  
319 as for the flash responses described above and computed response peak latencies for each stimulus condition.  
320 The latencies were then averaged across the two motion directions.

321 *Latency estimation in control experiment.* In the control experiment, we computed response peak latencies for  
322 flashes from arrangement A1 and for moving bars from arrangement A2 (see section *Control Experiment*  
323 above). To compute flash response latency for a given spatial offset, we first selected multiunits whose  
324 receptive field centers were within the spatial extent of the presented flash. Response peak latency was then  
325 extracted from this set of multiunits as described under the section *Estimation of flash response peak latency*.  
326 To compute the motion response latency for any spatial offset, we first selected multiunits whose receptive field  
327 centers were within the spatial extent of the moving bar when it hit the ARFC. Since the flashes were presented  
328 at different horizontal locations when the moving bar hit the ARFC, the same set of multiunits were used for  
329 extracting latencies under different spatial offsets. Motion response peak latencies were then computed as  
330 described under the section *Estimation of motion response peak latency*. Note that we chose to include a spatial  
331 offset for analysis only if there were more than ten multiunits for that condition. With this criterion, only the  
332 three spatial offsets around the ARFC qualified.

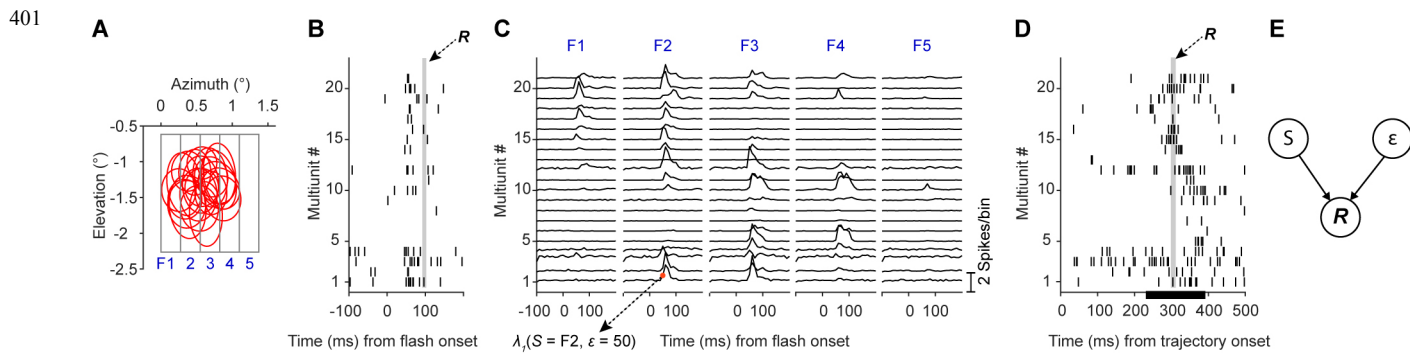
333 *Statistical analysis.* All the statistical analyses on the neural data were done by bootstrapping (Efron and  
334 Tibshirani 1994). From the response (averaged over multiunits) peak latencies of flash and moving bar under  
335 various conditions, we computed the following test statistics: latency difference between flash and moving bar  
336 (**Fig. 7B, Fig. 12-Fig. 13, F**); slope of the trend in the latencies (**Fig. 7B, Fig. 12-Fig. 13, F**); latency differences  
337 and perceived spatial offset equivalents when changing speed (**Fig. 7C & D, Fig. 10E & F, Fig. 12-Fig. 13, G &**  
338 **H**) and luminance (**Fig. 9C, F & G, Fig. 10H & I, Fig. 14G-I**); and for the control experiments: latency  
339 differences across multiple spatial offsets (**Fig. 11B**); latency differences for stimuli presented in isolation versus  
340 in combined condition (flash and moving bar presented together) (**Fig. 11C**). To obtain significance levels and  
341 confidence intervals on these test statistics, we repeated 2000 times the entire procedure that generated a test  
342 statistic, each time with a different random set of multiunits obtained by resampling with replacement. Since the  
343 electrodes were implanted chronically, individual recordings from different days may not represent independent  
344 samples. To ensure that we use only independent samples for bootstrapping, we sampled electrode identities  
345 and included all units obtained from sampled electrodes. This procedure estimates the unit-to-unit variability  
346 without being confounded by dependent samples due to chronic recordings. From this bootstrap distribution, we  
347 computed the 95% percentile confidence intervals, which are reported as error bars. We defined the significance  
348 level (p-value) as  $p = 2 \min(q, 1 - q)$ , where  $q$  is the percentile of zero under the bootstrap distribution (this  
349 analysis assumes that the bootstrap distribution is an appropriate measure of the variability under the null  
350 hypothesis).

351 *Human psychophysics: task.* Two human subjects (authors MS and SP) performed the standard flash lag  
352 psychophysical experiment as described previously (Subramaniyan et al. 2013). The subjects sat in a dark room  
353 with their heads stabilized by a chin-rest. After the subjects dark-adapted their eyes for five minutes, the  
354 stimulus presentation began. The subjects were simply instructed to stay fixated at the fixation spot during  
355 stimulus presentation; their eye movements were not tracked. In any given trial, we presented a flash below  
356 another bar that moved from left to right; the gap between the bottom edge of the moving bar and top edge of  
357 the flashed bar was  $0.3^\circ$  and both bars had identical luminance. We used seven different horizontal offsets  
358 between the flash and moving bar centers. The offset values ranged from around  $-6.3^\circ$  to  $2.4^\circ$  in steps of around  
359  $1.5^\circ$ . We used a constant flash location and created the spatial offsets by choosing the time of flash relative to  
360 the instantaneous position of the moving bar. To be comparable to the physiological experiments with monkey  
361 L, we made sure that at zero spatial offset, the average position of the flash and moving bar centers matched the  
362 ARFC used for monkey L. In each session, we randomly interleaved four bar luminance values. These  
363 luminance values, bar dimensions, monitor background luminance and speed of the moving bar were identical  
364 to those used in the luminance modulation experiment with monkey L, although here a longer motion trajectory  
365 of  $18^\circ$  was used. Using a keyboard, the subjects reported if the leading edge of the moving bar was on the right  
366 or left side of the flash at the moment the flash appeared. The subjects completed a total of seven sessions (MS:  
367 5, SP: 2). In most sessions, we presented a total of 28 stimulus conditions ( $7$  offsets  $\times$   $4$  luminance values  $\times$   $1$   
368 motion direction  $\times$   $1$  speed). Each condition was repeated 20 times giving about 560 trials per session. Each  
369 session lasted for an average 23 min.

370 *Estimation of perceived spatial offset:* To quantify the perceived spatial offset, we first converted the subjects'  
371 responses into a probability of reporting that the moving bar was ahead of the flash. Then we fitted a logistic  
372 function to these probabilities as a function of spatial offsets, using psignifit3.0 toolbox (Fründ et al. 2011;  
373 Wichmann and Hill 2001a; b). In the toolbox, we chose the constrained maximum likelihood method for  
374 parameter estimation and parametric bootstrapping for estimation of confidence intervals for parameters. We  
375 constrained the upper and lower asymptotes of the psychometric function to be equal with the prior distribution  
376 being a uniform distribution on the interval [0 0.1]. We defined the perceived spatial offset as the point of  
377 subjective equality, that is the veridical spatial offset at which subjects reported that the moving bar was ahead  
378 or behind the flashed bar with equal probability. To examine how the perceived spatial offset changed with  
379 luminance, we pooled the responses across sessions for each bar luminance before fitting the psychometric  
380 function. To perform statistical tests however, we fitted psychometric function for each session separately and  
381 computed perceived spatial offset.

382 *Statistical analysis of psychophysical data.* For all statistical test on psychophysical data, linear mixed models  
 383 were constructed in the statistical software PASW-18, with the following common settings: subjects were  
 384 treated as random effects and perceived spatial offset as dependent variable. Specifically, the slope of the trend  
 385 of the perceived spatial offset as a function of bar luminance (**Fig. 9E**) was tested for significance using the bar  
 386 luminance as a covariate with the session start times set to indicate repeated measures. To test the effect of  
 387 motion condition (foveopetal versus foveofugal) and speed on the perceived lag (**Fig. 10B & D**), speed was  
 388 used as a covariate and motion condition as a factor, with the combination of motion condition and session start  
 389 times set to indicate repeated measures.

390 *Probabilistic population decoding.* The decoding method used here was chosen for its simplicity and its suitability for  
 391 our experimental conditions abstracting away from neuronal implementation level details. Our goal was to decode the  
 392 stimulus position presented to the animal from the single- or multiunit population activity based on the  
 393 framework of probabilistic population coding (Dayan and Abbott 2005; Ma et al. 2006; Zhang et al. 1998). We  
 394 took advantage of the fact that the motion stimulus we used was essentially a sequence of flashes. Hence, to  
 395 decode the moving bar location, we first model the spatial encoding by measuring the population activity for  
 396 the different flashed locations of the bar. Then, when the moving bar was presented, we decoded its  
 397 instantaneous position by identifying the bar stimulus that was most likely, given the population activity at  
 398 that instant. Note that in our experiments, only part of the motion trajectory overlaps with the space covered by the  
 399 flashes. Since the spatial encoding is based on flash responses, we restricted the motion decoding to the region of the  
 400 trajectory overlapping the flash locations. The decoding method is formalized as follows.



401 **Fig. 3.** Probabilistic population decoding. **A**, Outlines of receptive fields (red) of simultaneously recorded multiunits ( $n =$   
 402 21) from a single representative session from monkey CL. The gray rectangles show the outlines of different flashes  
 403 (labeled at F1, 2, 3, 4, 5) presented one at a time. **B**, Single-trial raster plot of spiking responses (dark vertical bars) of all  
 404 multiunits in **A** to a flash (F2). The spike counts within the thin gray vertical box (of width  $\Delta t = 10$  ms) forms the activity  
 405 vector (**R**) used in the decoding procedure. **C**, Mean spike count across trials in 10 ms consecutive time bins for all  
 406 multiunits under each flash condition indicated on the top of each panel. An example value for  $\lambda_i(S, \varepsilon)$  parameter (see main  
 407 text) is indicated at the bottom left. The ordinate scale bar for the traces is shown on the bottom right corner. **D**, Single-trial  
 408 raster plot of spiking responses (dark vertical bars) of all multiunits in **A** to a bar moving from left to right at a speed of 7/s.  
 409 Vertical thin gray rectangle as in **B**. The black horizontal bar on the abscissa marks the time period the moving bar spent  
 410 within the flashed region shown in **A**. **E**, Graphical model of population activity. The population neural response at a given  
 411 time bin (**R**) is governed by the stimulus (**S**) and the time elapsed (**ε**) since stimulus onset.

412 A flashed stimulus (**Fig. 3A**) evokes neural activity that extends over time outlasting the presence of the  
 413 stimulus (~10ms) on the monitor (**Fig. 3B**). The post-stimulus period can be split into a sequence of contiguous  
 414 time bins (of width  $\Delta t$ ). We assume that, conditioned on the stimulus, the spiking responses are independent  
 415 across both time and neurons. That is, activity (**R**) in any given time bin depends only on the stimulus location  
 416 (**S**) and the elapsed time since stimulus onset (**ε**). Under this assumption, the neurons spike according to

419 independent inhomogeneous Poisson distribution, with a time- and neuron-dependent mean spike count  
 420 parameter  $\lambda$  (**Fig. 3C**). This produces the following probability distribution for neural activity ( $\mathbf{R}$ ) in a  
 421 single time bin of width  $\Delta t$ :

$$p(\mathbf{R} | S, \varepsilon) = \prod_{i=1}^N p(n_i | S, \varepsilon) = \prod_{i=1}^N e^{-\lambda_i(S, \varepsilon)} \frac{\lambda_i(S, \varepsilon)^{n_i}}{n_i!} \quad (1)$$

422 where

423 S - Stimulus (bar) at one of M possible locations (for example, see gray rectangles in **Fig. 3A**).  
 424

$\varepsilon$  - Time elapsed since stimulus onset.

425 N - Number of neurons simultaneously recorded.

426  $n_i$  - Spike count in a given time bin of width  $\Delta t$  for neuron  $i$ .

427  $\lambda_i(S, \varepsilon)$  - Mean spike count of neuron  $i$  in a time bin of width  $\Delta t$  after a delay of  $\varepsilon$  from stimulus (S) onset at  
 428 one of M possible locations.

429  $\mathbf{R}$  -  $(n_1, n_2, \dots, n_N)$  - population activity (spike counts) in a single time bin.

430

431 Note that, for the flash-evoked neural activity in any given time bin, the experimenter knows which flash  
 432 stimulus caused the activity and how much time has elapsed since the stimulus onset (**Fig. 3B**). However, these  
 433 two parameters are unknown from the brain's perspective. In the case of the moving stimulus for which *a*  
 434 *priori* we do not know the response latency, even the experimenter cannot know which stimulus location  
 435 causes neural activity in a given time bin (**Fig. 3D**). This is due to the moving bar changing its location in every  
 436 time bin leading to essentially multiple stimulus locations driving the neural activity in different time bins. As  
 437 the experimenter cannot know which stimulus location caused the activity, he/she also cannot know how much  
 438 time has elapsed since the onset of the stimulus (at a given location) driving the activity. For these reasons, in  
 439 our decoding of flashed and moving stimuli, we treat the stimulus location and time elapsed since stimulus  
 440 onset/arrival at a given location as random variables that follow a uniform distribution with flat priors. Note  
 441 that the response at a single time bin for a moving stimulus is likely driven by *multiple* stimulus (bar) locations  
 442 (spatiotemporal integration). However, to decode this activity, we are using an encoding model where  
 443 population activity at each time arises from *single* stimulus (flash) locations. Hence in our decoding procedure,  
 444 we are only approximating the spatiotemporal integration involved in generating population activity during  
 445 motion. This leads to a graphical model (**Fig. 3E**) which, in combination with *Eq. 1*, can be used to decode the  
 446 stimulus position from the neural activity. Decoding this way in small time bins ( $\sim 10$ ms) implies that a rate  
 447 code is used by the brain for computing stimulus position. To compute the probability of a stimulus given the  
 448 population activity in a single time bin, we first derive a joint distribution based on the model in **Fig. 3E**.

449

$$p(S, \varepsilon, \mathbf{R}) = p(S)p(\varepsilon)p(\mathbf{R} | S, \varepsilon) \quad (2)$$

450 We assumed S and  $\varepsilon$  follow a uniform distribution (range of S: horizontal extent of flashed region, range of  $\varepsilon$ :  
 451 10 to  $\sim 175$ ms) and hence  $p(S)$  and  $p(\varepsilon)$  are constants (flat priors). We can then marginalize the above joint  
 452 distribution over the elapsed time  $\varepsilon$  to compute the probability of a stimulus location given the population  
 453 activity  $\mathbf{R}$  in any arbitrary time bin:

454

$$p(S, \varepsilon | \mathbf{R}) = \frac{p(S, \varepsilon, \mathbf{R})}{p(\mathbf{R})} = \frac{p(S)p(\varepsilon)p(\mathbf{R} | S, \varepsilon)}{p(\mathbf{R})} \quad (3)$$

$$p(S | \mathbf{R}) = \sum_{\varepsilon} p(S, \varepsilon | \mathbf{R}) = p(S) \sum_{\varepsilon} p(\varepsilon) \frac{p(\mathbf{R} | S, \varepsilon)}{p(\mathbf{R})} \quad (4)$$

455

456 As  $p(S)$  and  $p(\varepsilon)$  are assumed to be constants for all values of  $S$  and  $\varepsilon$  respectively, they can be absorbed  
457 along with  $p(\mathbf{R})$  into the normalization constant  $Z(\mathbf{R})$  simplifying *Eq.4* as:  
458

$$p(S | \mathbf{R}) = \frac{1}{Z(\mathbf{R})} \sum_{\varepsilon} p(\mathbf{R} | S, \varepsilon) \quad (5)$$

459  
460 where  $Z(\mathbf{R})$  can be computed using the following normalization constraint:  
461

$$\sum_{j=1}^M p(S_j | \mathbf{R}) = 1 \quad (6)$$

462 where the subscript  $j$  indexes the possible positions of the bar stimulus in visual space. Since the decoding was  
463 restricted to the space occupied by the flashes, the above constraint (*Eq. 6*) is justified as the decoded position  
464 should be within the flashed space. By using the above constraint, we avoided computing  $p(\mathbf{R})$  explicitly,  
465 as done by previous studies in similar decoding problems (Sanger 1996; Zhang et al. 1998). Note that for  
466 monkeys A and CH, although 7 flashes were presented in the task, we only included the central 5 flashes in the  
467 analysis as the flashes at the periphery did not have sufficient receptive field coverage.  
468

469 Decoding was done trial by trial for each recording session using neurons recorded simultaneously. The same  
470 number of trials was used for all stimulus conditions within a session. In each trial, from stimulus onset, we  
471 stepped forward in small contiguous (non-overlapping) time bins ( $\Delta t$  = monitor refresh period, 8.3 ms for  
472 monkey L, 10 ms for others) and computed the posterior probability of each of the possible stimulus  
473 positions ( $M$  in total), given the population activity at that time bin. Hence, at every time instant, for a  
474 given test stimulus (flash or moving bar), we get an  $M$ -element vector of posterior probabilities that sum up to  
475 1. For all stimulus conditions, the posterior probability was assigned to the end of the time bins. For example,  
476 the probability computed in the [0, 10) ms time bin was assigned to  $t = 10$ . This ensures that probability is  
477 causally related to the population activity. Also, note that for the speed of 7%, only every fifth moving bar  
478 center matched flash centers (**Fig. 5A**). Hence when computing  $\lambda_j(S, \varepsilon)$ , we interpolated the mean firing  
479 rate from the flash centers to all positions ( $M$  in total) that the moving bar center occupied (white dots in  
480 panel D of **Fig. 12-Fig. 14**). For simplicity, the same interpolated  $\lambda_j(S, \varepsilon)$  was used for all speeds. For the  
481 luminance modulation experiment, a similar interpolation procedure was done and the decoding of bar stimuli  
482 of a given luminance was based on encoding obtained from responses of flashes of matching luminance.  
483

484 For the marginalization in *Eq.4*, we chose a time window that covers the flash-evoked responses of all  
485 recorded neurons for all monkeys. Based on visual inspection of the neural responses, this window was set to  
486 10-175ms for monkey L (to allow for longer response latencies at low luminance conditions, see **Fig. 8**) and  
487 10-150 ms for all other monkeys (see **Fig. 6**). The results and conclusion based on decoding are not sensitive  
488 to the exact values of the above time windows. For example, shortening the above windows to 20-130ms and  
489 20-100ms respectively does not change the results and conclusions presented. However, including some time  
490 bins in which the population activity is at the baseline level minimizes the “edge effect” where the decoder,  
491 when decoding baseline-level activity, assigns a relatively higher probability to stimulus locations at the  
492 periphery (“edge”) of the flashed region (see the decoding in the 0-50ms window in **Fig. 14B**). This effect  
493 arises because the edge regions often have relatively poor receptive field coverage in our dataset (see first and  
494 last gray rectangle in **Fig. 14A**). When a bar stimulus is presented here, it evokes a population response which  
495 is similar to the baseline activity (see **Fig. 3C**, stimulus F5). Consider a decoder that does not include any  
496 baseline-level time bins in the marginalization time window in *Eq. 5*. When this decoder decodes baseline-  
497 level activity from any stimulus condition, it will assign a higher posterior probability to the edge regions  
498 (edge effect) as the bar stimuli at the interior locations are unlikely to evoke such poor baseline-level activity.  
499

500 Instead, including some baseline bins (e.g. bins with  $\epsilon = 10 - 30\text{ms}$ ) in the marginalization time window  
501 minimizes this effect. This is because, these bins contribute appreciably to the likelihood term inside the  
502 summation operation in *Eq. 5*. Hence, for a given  $S$ , the total likelihood summed over  $\epsilon$  ( $\sum_{\epsilon} p(S|R, \epsilon)$ ) will be  
503 higher compared to when not including these bins. Moreover, as the baseline activity is similar for all bar  
504 locations ( $S$ ), the large likelihood contribution will also be similar for all  $S$ . The result of such an overall  
505 increase in the total likelihood is that, after normalization in *Eq. 5* (division by  $Z(R)$ ), the posterior  
506 probabilities of the  $M$  locations become similar at times when there is no stimulus evoked activity, thereby  
507 minimizing the edge effect.

508  
509 *Cross-validation.* The decoding was done on individual trials. Note that in the above model, we learnt the  
510 spatial encoding from the population response to flashes. Hence, when we decoded flash stimuli, to prevent  
511 overfitting, we kept aside a given trial for testing and used the remaining trials to train the model (i.e., compute  
512 the  $\lambda$ 's). This was then repeated for all available trials. For decoding the motion stimulus however, the  
513 separation into training and testing trials was unnecessary because the trials used for training (flash trials)  
514 were different from the trials in which testing was done (motion trials).

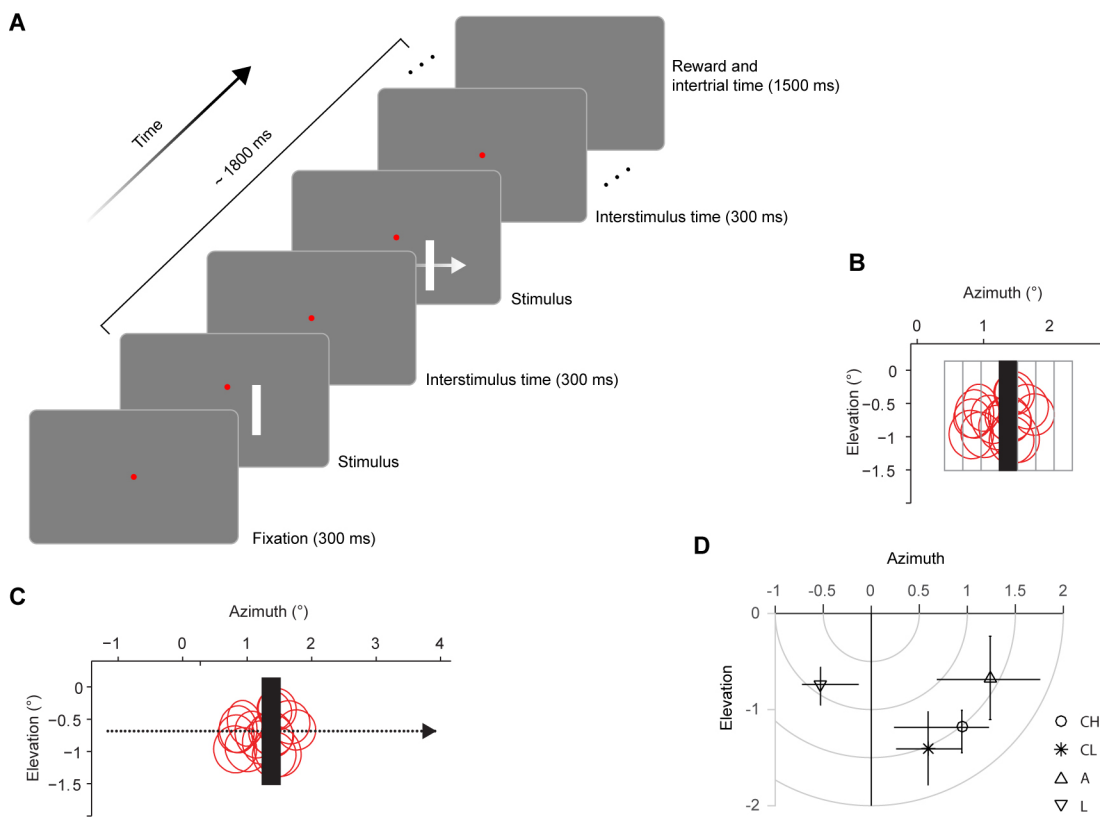
515  
516 *Computing latencies from probabilistic decoding.* The posterior probabilities of bar locations computed as  
517 described above were first averaged across trials and then across sessions for a given monkey. For  
518 estimating the decoding latency for flashes, we first averaged the probability values corresponding to positions  
519 within the horizontal spatial extent (see white horizontal bar in panel B top in **Fig. 12-Fig. 14**) of a flash stimulus.  
520 This was repeated for each flash condition and then the probabilities were averaged across the flashes (**Fig. 12-**  
521 **Fig. 14, C**) and smoothed with a Gaussian kernel with a standard deviation of  $\sim 5$  ms. We then computed the  
522 latency of the peak of this averaged posterior probability as a measure of the latency of flash stimulus  
523 representation (**Fig. 12-Fig. 14, F**). For motion latency, first we aligned (centered) the probability vector  
524 computed at each time bin to the moving bar's instantaneous position. We included time bins starting from the  
525 time the moving bar entered the flashed zone until about 120 ms or less after the bar exited the flashed region of  
526 space to account for latency of responses. The aligned vectors were then averaged (**Fig. 12-Fig. 14 E**) and  
527 smoothed with a Gaussian kernel with a standard deviation of  $0.1^{\circ}$ , the distance between the peak of the  
528 posterior probability and the origin, was taken as the spatial lag of the moving bar representation. The time  
529 delay (latency) corresponding to this spatial lag was then calculated by dividing the spatial lag by the speed of  
530 the moving bar. To obtain significance levels and confidence intervals on test statistics based on latencies  
531 computed as above, we repeated 2000 times the entire decoding procedure that generated a test statistic, each  
532 time with a different random set of single or multiunits within each session, by resampling with replacement.  
533

## 534 Results

535 We assessed if there are differences in the representation delays (latencies) of moving and flashed stimuli and  
536 whether this could account for the perceived spatial misalignment (offset) in the flash lag illusion. To this end,  
537 we recorded neural activity from V1 while the monkeys were shown either a flashed or a moving bar in a  
538 passive fixation task (**Fig. 4A**, see Methods). We performed two experiments: In the first, we varied the  
539 direction of motion and speed of the moving bar (7, 14 or 28  $^{\circ}/\text{s}$ ), while keeping the moving and flash stimuli at  
540 a fixed luminance (23 or 36  $\text{cd}/\text{m}^2$ ). In the second, we kept the speed constant and manipulated the luminance of  
541 the flash and the moving bar. In both cases, we measured the effect of the manipulation on the latency  
542 difference between the moving and the flashed bar and compared it to the psychophysical results from monkeys  
543 (Subramanyan et al. 2013) and humans (Murakami 2001; Purushothaman et al. 1998; Subramanyan et al.  
544 2013; Whitney et al. 2000; Wojtach et al. 2008).

545 For experiment 1, we recorded from 523 multiunits in three animals using chronically implanted tetrode arrays.  
546 For experiment 2, we collected responses of 256 multiunits in one animal, using a 96-channel Utah array. After  
547 an initial receptive field mapping session, the main task began. We presented bright bars on a gray (experiment

548 1) or dark (experiment 2) background. In each trial either a flash or a moving bar was shown. Since we recorded  
 549 from many neurons simultaneously, the flash locations were not optimized for any particular neuron. Instead, in  
 550 each recording session, flashes were shown at five to seven fixed locations covering the receptive fields of all  
 551 the recorded neurons (**Fig. 4B**). The moving bar swept across the receptive fields horizontally at a constant  
 552 speed from left to right or from right to left with equal probability (**Fig. 4C**). For experiments 1 and 2, the  
 553 receptive fields of units were in the right and left hemifield respectively (**Fig. 4D**). To test the predictions of  
 554 different models of flash lag illusion, we estimated the stimulus representation delays of flashed and moving  
 555 bars in V1 using two different approaches. The first method was based on the neuronal responses recorded on  
 556 individual recording sites and the second one was based on decoding simultaneously recorded single- and  
 557 multiunit population activity. Specifically, we tested the dependence of the latency difference between flashed  
 558 and moving stimuli on speed, luminance and direction of motion.



559

560 **Fig. 4.** Fixation task and stimuli. **A**, Monkeys fixated their gaze at a red circular dot at the center of the monitor within a  
 561 fixation radius of 0.6°. After they maintained fixation for 300 ms, a single randomly chosen bright flash or moving  
 562 stimulus was presented in a gray or dark background. The stimulus offset was followed by a 300 ms period in which no  
 563 stimulus was presented except for the fixation spot. Then a randomly chosen flash or moving bar was presented again.  
 564 With the monkeys maintaining fixation, this cycle continued until at most 1800 ms elapsed, after which they obtained a  
 565 squirt of juice as reward. The next trial started after an inter-trial period of 1500 ms. **B**, A flash (black bar) was presented at  
 566 one of five to seven adjoining locations (gray rectangles) tiling the receptive fields (red circles) of all recorded neurons. **C**,  
 567 The moving bar (black bar) had the same size as the flash and moved from left to right or from right to left. The dots  
 568 denote the positions of the bar center along the entire trajectory as the bar moved from left to right at a speed of 7 °/s. In **B**  
 569 and **C**, the coordinate (0° Azimuth, 0° Elevation) marks the center of fixation and the bars and receptive field outlines are  
 570 drawn to scale. Note that the red circles show the outlines of only a subset of the recorded neurons. **D**, Markers show  
 571 median of receptive field centers of monkeys (CH, CL, A and L). The horizontal and vertical error bars indicate 95%  
 572 percentile limits of azimuth and elevation respectively of receptive field centers. Isoeccentricity lines are shown in gray.

573 **Dependence of latency difference on bar speed**

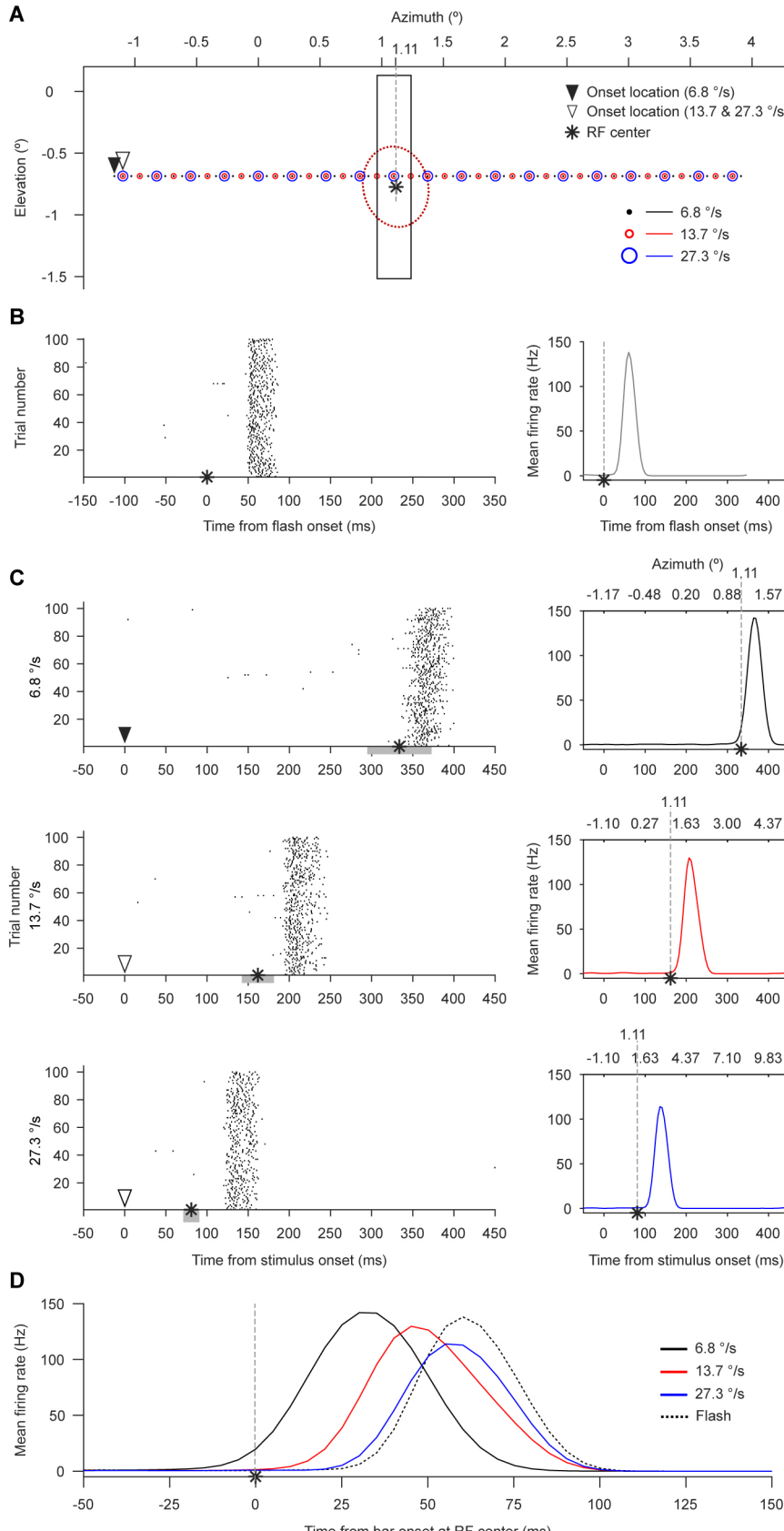
574 We asked if the latency difference between the responses to flashed and moving bars depends on the speed of  
575 the moving bars. To this end, we recorded neural activity when a flash or a moving bar was presented and  
576 estimated response peak latencies using the receptive field (RF) center as a reference location (**Fig. 5A**). We  
577 then asked how long does the neuron take to reach its peak firing rate for a bar that is flashed at this location  
578 and for the same bar at the same location when it is part of a motion trajectory (**Fig. 5A**). For both stimuli, the  
579 time of response peak with respective to the time at which the bar appears (flash, **Fig. 5B**) or arrives (motion,  
580 **Fig. 5C**) at the same reference location, was taken as their respective representation delays (**Fig. 5D**). The  
581 assumptions behind using response peaks for computing representation delays are described in the Methods  
582 section. Note that when the speed increases, the time required for the bar to arrive at the reference location  
583 decreases (**Fig. 5D**). However, this difference in bar arrival times does not add to motion latencies as we  
584 measured latency after all stimuli arrive at a common reference location. The center of the receptive field is  
585 operationally defined as the region that elicits maximal response. Assuming an RF-based labeled-line code  
586 common for flashed and moving stimuli, if both stimuli are processed with the same delay, then, when either  
587 the moving or the flashed bar is at the RF center, they should both elicit their respective maximal response with  
588 the same delay. In other words, when the moving bar arrives at the RF center one would expect a peak response  
589 to occur with the same delay, because at that instant, the moving bar is indistinguishable from a flash. In  
590 contrast, we find that the response peak for all three moving stimulus conditions occurs earlier compared to that  
591 of flash (**Fig. 5D**). In addition, as the speed increases, the response peak latency also increases and approaches  
592 that of the flash. These observations suggest that a moving stimulus is processed differently from a flashed one  
593 and is represented earlier in time in a speed dependent manner compared to a flash in the same location.

594 To estimate latency at the population level, we chose to first average the responses across the multiunits and  
595 then compute response peak latency from this average rather than vice versa. This was done because some  
596 multiunit responses had multiple response peaks, making it unclear as to which peak should be considered for  
597 latency estimation, and in experiment 2, the individual unit responses were too weak (**Fig. 8**) at the lowest  
598 luminance values to reliably find the response peak. Averaging the responses over the multiunits first, enabled  
599 us to robustly estimate latency and to apply a single procedure uniformly across all stimulus conditions.

600 Across our sample of multiunits from each monkey (**Fig. 6**), the peak response latencies for the motion  
601 condition at all three speeds were shorter compared to those for flashes (**Fig. 7A & B**; for each monkey,  $p <$   
602 0.0005, Bonferroni corrected, bootstrap test; see Methods). As the speed increased, the latency of the motion  
603 response approached that of the flash (**Fig. 7B**). Therefore, the latency difference between flash and motion  
604 decreased as the speed increased (**Fig. 7C**;  $p < 0.0005$ , bootstrap test) but remained greater than zero ( $p <$   
605 0.0005, Bonferroni corrected; bootstrap test).

606

607

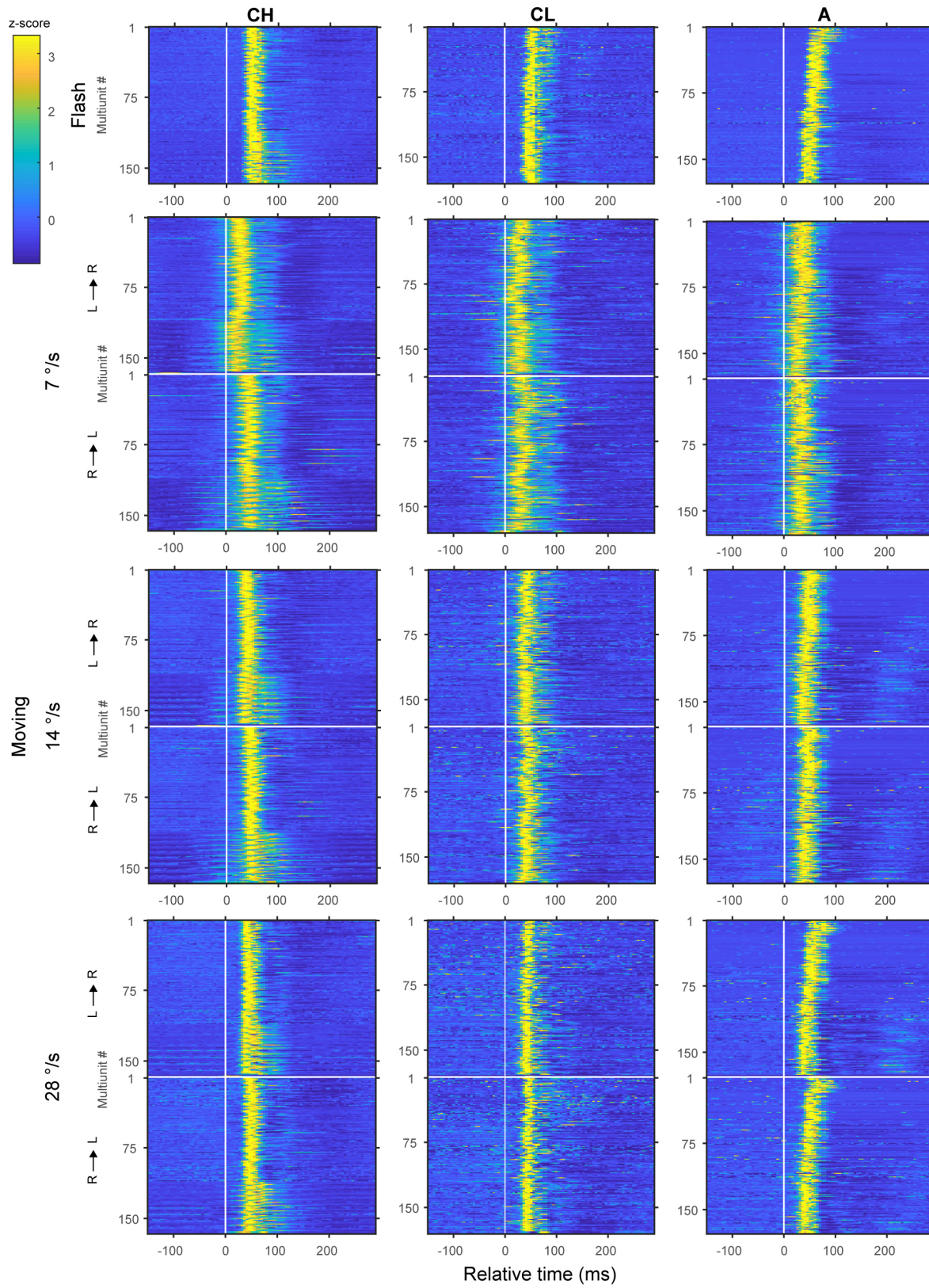


609 **Fig. 5.** Single neuron responses to flash and moving bar and estimation of response peak latencies. **A**, Illustration (drawn  
610 to scale) of the bar stimulus (rectangle) in visual space. The red dotted circle shows the 2-standard deviation outline of the  
611 neuron's (from monkey A) receptive field (RF) with the RF center marked by the asterisk. In all panels of this figure, the  
612 vertical gray dashed line refers to the azimuth ( $1.11^\circ$ ) of RF center. In the flash condition, the bar is presented for one  
613 video frame as depicted. For moving conditions, the bar center occupies sequential positions marked by black dots  
614 ( $6.8^\circ/\text{s}$ ), small red circles ( $13.7^\circ/\text{s}$ ) or large blue circles ( $27.3^\circ/\text{s}$ ); the bar shown is the instantaneous moving bar position  
615 that matches the flash. The triangles indicate the starting position of moving bar. **B**, Left, raster plot showing neural  
616 responses to the flash shown in **A**, aligned to stimulus onset time. Each dot denotes a spike and each row is a trial (only a  
617 subset of trials is shown). Right, mean firing rate plot for flash. **C**, Left column, raster plots of responses for the bar moving  
618 from left to right at speeds indicated on the ordinate. Response times are aligned to motion trajectory onset time marked by  
619 the triangles. The gray horizontal bars mark the time needed to traverse the horizontal spatial extent of the receptive field  
620 outline shown in **A**. Right column, mean firing rate plots corresponding to the respective raster plots shown on the left. In  
621 all subpanels of **C**, the time at which the moving bar center crosses the receptive field center is marked by the asterisk. **D**,  
622 Mean firing rate responses to all stimuli. Flash response is aligned to flash onset time. Moving bar responses are aligned to  
623 the time (asterisks in **C**) at which the moving bar center crosses the receptive field center. The latency of response peaks for  
624 flash and moving bars is computed from this plot.

625

626

627



629 **Fig. 6.** Trial-averaged responses of multiunits in the speed manipulation experiment in monkeys (CH, CL and A).  
630 Columns of panels represent monkey subjects indicated on the top. Rows of panels represent stimulus conditions indicated  
631 on the left. In each image, each row, ordered in ascending order of recording day, represents response of a multiunit. The  
632 vertical white line marks the time the stimulus hits the receptive field center. The horizontal white line separates the two  
633 motion direction conditions: L→R, motion from left to right; R→L, motion from right to left. Color range is clipped at  
634 95<sup>th</sup> percentile of responses grouped from all conditions.

635 This effect is consistent with the speed dependence of the magnitude of the perceived spatial offset observed in  
636 the psychophysical data collected in macaques (Subramaniyan et al. 2013). In our electrophysiological  
637 experiments, we manipulated the speed and measured the representation latencies of flash and moving bar  
638 rather than the perceived spatial offset which cannot be computed directly from the neural responses since it is a  
639 subjectively perceived quantity. In the psychophysical test, the subjects report the relative spatial offset between  
640 the flash and moving bar rather than how far the moving bar lags behind its own veridical location. Hence in  
641 computing the neural equivalent of perceived spatial offset, the latency of moving bar alone cannot be used - it  
642 is the difference ( $L_d$ ) in the representation delays of flash ( $L_f$ ) and moving bar ( $L_m$ ) that is needed. The neural  
643 equivalent of perceived spatial offset ( $X$ ) was then computed by multiplying the speed ( $v$ ) by the latency  
644 difference, i.e.,

$$X(v) = v \cdot L_d = v \cdot (L_f - L_m) \quad (7)$$

645

646 Although the latency difference decreased with speed, the perceived spatial offset equivalent increased with  
647 speed (**Fig. 7D**;  $p < 0.0005$ , bootstrap test). This counterintuitive effect can be explained by noting that the  
648 latency difference is not a constant but varies with speed (**Fig. 7B**). Hence,

$$X(v) = v \cdot (L_f - L_m(v)) \quad (8)$$

Differentiating both sides with respect to speed,

$$\frac{dX(v)}{dv} = L_f - \left( v \cdot \frac{dL_m(v)}{dv} + L_m(v) \right) \quad (9)$$

From *Eq. 9*, for the perceived spatial offset to increase with speed, i. e, for  $\frac{dX(v)}{dv} > 0$ ,

$$\begin{aligned} L_f - \left( v \cdot \frac{dL_m(v)}{dv} + L_m(v) \right) &> 0, \quad \text{or} \\ L_f &> \left( v \cdot \frac{dL_m(v)}{dv} + L_m(v) \right) \end{aligned} \quad (10)$$

649

650 Hence, as long as *Eq. 10* is satisfied, the perceived spatial offset will increase with speed even if motion latency  
651 increases ( $\frac{dL_m(v)}{dv} > 0$ , our data) or decreases ( $\frac{dL_m(v)}{dv} < 0$ ) with speed.

652 The simplest case arises when motion latency does not change with speed ( $\frac{dL_m(v)}{dv} = 0$ ), that is,

$$L_m(v) = L_m$$

$$L_f - L_m = c, \quad \text{where } c \text{ is a constant}$$

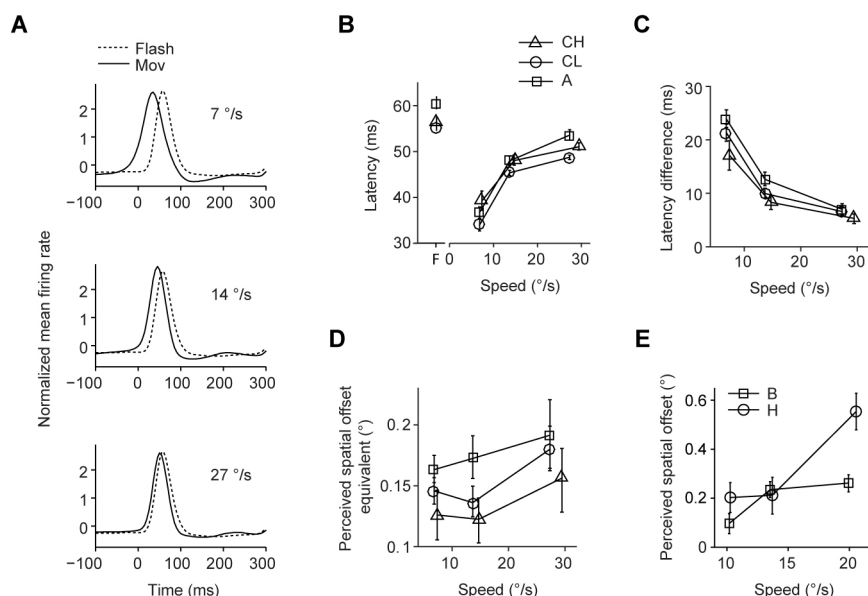
Therefore,

$$X(v) = v \cdot c \quad (11)$$

653

654 Hence Eq.11 shows that perceived spatial offset linearly increases with speed as long as  $L_f > L_m$ . This  
 655 assumption of constant motion latency is commonly made in psychophysical literature of flash lag illusion.  
 656 Consistent with this assumption, some psychophysical studies have shown that the perceived spatial offset  
 657 increases with speed (see Discussion). However, as indicated by Eq.10, this assumption is not necessary for  
 658 explaining the increase in perceived spatial offset with speed. Our results demonstrate that despite an increase in  
 659 motion latency with speed (Fig. 7B), the neural equivalent of perceived spatial offset increases with speed (Fig.  
 660 7D).

661 The increase of the perceived spatial offset equivalent with speed is consistent with our psychophysical results  
 662 (Subramaniyan et al. 2013) from two other monkeys of the same species (Fig. 7E) and with human  
 663 psychophysical studies (see Discussion). Together, these results show that in primary visual cortex, irrespective  
 664 of the speed, the moving bar latency is not fully compensated (zero latency) as would be predicted by the spatial  
 665 extrapolation model and that the latency of flash and moving bar are not equal as would be predicted by the  
 666 motion-biasing model. On the other hand, our results are consistent with the differential latency model.



667

668 **Fig. 7.** Population response and its correlation to flash lag psychophysics. **A**, Normalized multiunit responses to flash  
 669 (dotted trace) and motion (solid trace), averaged over all multiunits from monkey A (n = 177). The speed of motion is  
 670 indicated on the top right corner of each panel. **B**, Mean response peak latency for flash and motion plotted as a function of  
 671 speed, for the three monkeys (n = 177, 166 and 180 for A, CH and CL respectively). The latencies for flash are plotted at  
 672 the abscissa location marked by 'F'. Error bars: 95% bootstrap percentile-based plug-in estimate of confidence intervals  
 673 (note that most CIs are smaller than the markers). **C**, Mean latency difference (flash latency minus motion latency) as a  
 674 function of speed. Markers, sample size and error bars are as in **B**. **D**, Speed dependence of perceived spatial offset  
 675 equivalent computed from latency differences shown in **C**. Markers and error bars are as in **B**. **E**, Speed dependence of  
 676 perceived spatial offset measured from two separate monkeys (B and H), re-plotted here from Subramaniyan et al. (2013).

677

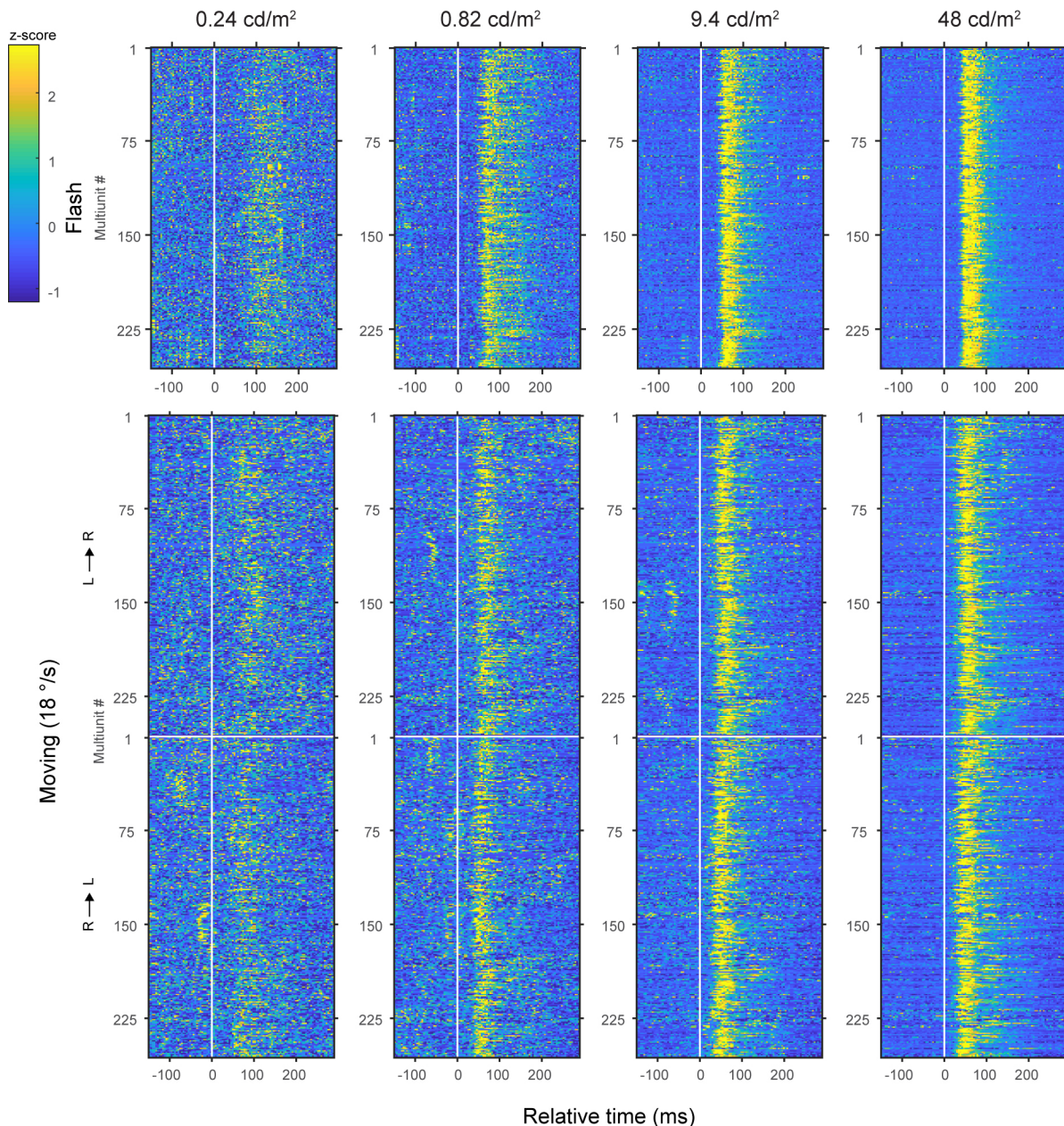
678

679

680 **Dependence of latency difference on bar luminance**

681 The latency difference between moving and flashed bars may also depend on bar luminance. To test this, in the  
682 second experiment, we fixed the speed of the moving bar at 18 °/s and presented flashes and moving bars with  
683 luminance values of 0.2, 0.8, 9 and 48 cd/m<sup>2</sup> (Fig. 8). We found that the motion response occurred earlier in  
684 time relative to the flash response (Fig. 9A). For all luminance values tested, the motion response peak latency  
685 was lower than that of the flash (Fig. 9B,  $p < 0.0005$ , Bonferroni corrected, bootstrap test). For both the flash  
686 and moving bar, the peak response latencies decreased as the luminance increased, although they decreased  
687 differently (Fig. 9B). Accordingly, the latency difference decreased as the luminance increased (Fig. 9C,  $p <$   
688 0.0005, bootstrap test).

689



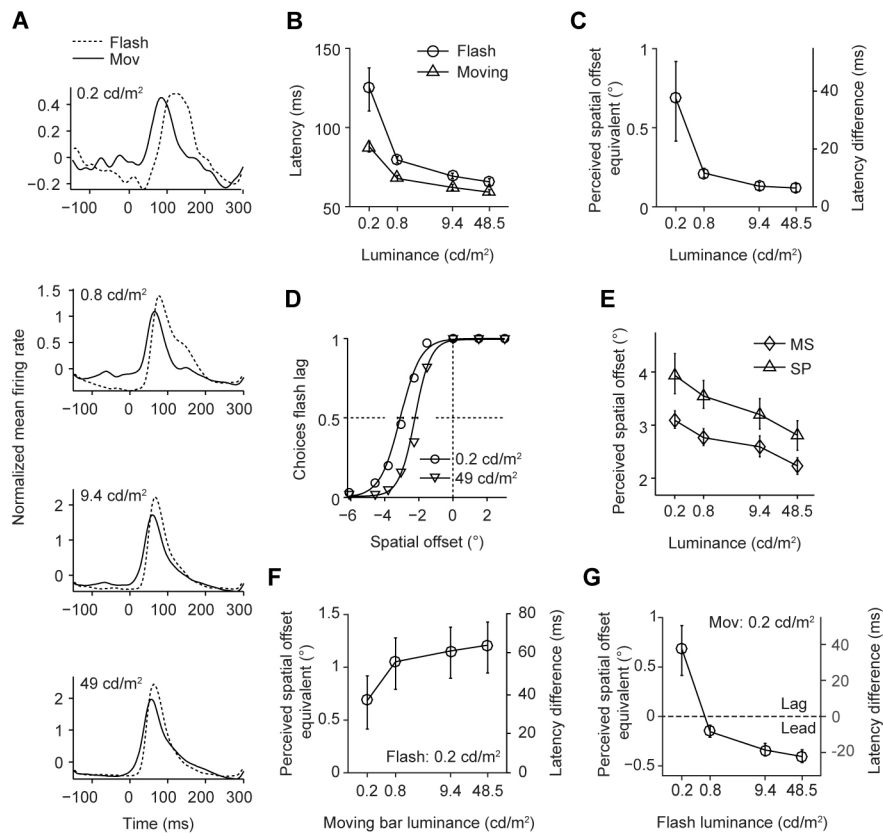
690

691 **Fig. 8.** Trial-averaged responses of multiunits in the luminance manipulation experiment in monkey L. Columns of panels  
692 represent stimulus luminance indicated on the top. Rows of panels represent other stimulus conditions indicated on the left.  
693 In each image, each row, ordered in ascending order of recording day, represents response of a multiunit. The vertical  
694 white line marks the time the stimulus hits the receptive field center. The horizontal white line separates the two motion  
695 direction conditions: L→R, motion from left to right; R→L, motion from right to left. Color range is clipped at 95<sup>th</sup>  
696 percentile of responses grouped from all conditions.

697

698 To compare physiological and psychophysical data, we again converted the latency differences into perceived  
699 spatial offset equivalent by multiplying the latency differences with speed (*Eq.8*). The perceived spatial offset  
700 equivalent decreased with luminance (**Fig. 9C**,  $p < 0.0005$ , bootstrap test). Although we currently do not have  
701 psychophysical data on the luminance dependence of the flash-lag effect in monkeys, we have previously  
702 shown that monkeys perceive the illusion similar to humans (Subramanyan et al. 2013). We therefore measured  
703 perceived spatial offsets from two human subjects using the same luminance and stimulus parameters used for  
704 the monkey physiology. Indeed, the perceived spatial offset decreased with luminance in both observers (**Fig.**  
705 **9D** and **Fig. 9E**;  $F(1, 24) = 14.6$ ;  $p = 0.001$ ; linear mixed model), in good agreement with the physiological  
706 results.

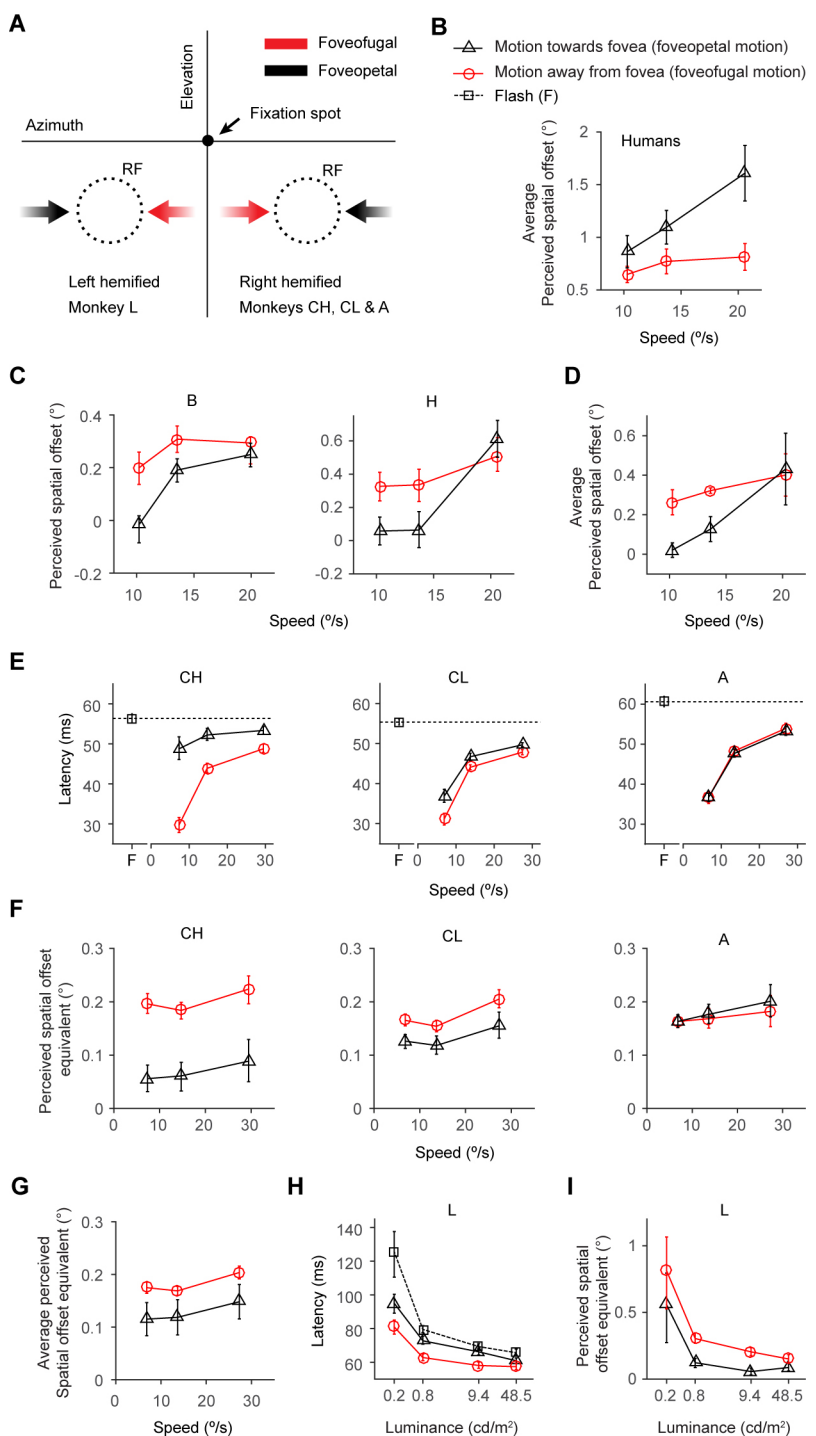
707 In the above analysis, we computed latency difference data between flash and moving bar with identical  
708 luminance and showed that they correlate well with human psychophysical data. Given that we presented each  
709 luminance condition in isolation, it is possible to compute the latency difference between a flash and a moving  
710 bar having different luminance values. In human psychophysics, when the flash luminance is fixed at a very low  
711 detectability level, the perceived spatial offset increases with the moving bar luminance (Öğmen et al. 2004;  
712 Purushothaman et al. 1998). To see if this is also evident in our neural data, we used the latency of the flash  
713 condition with the lowest luminance to compute latency difference at all moving bar luminance conditions.  
714 Interestingly, qualitatively similar to the human psychophysical results, we found that the perceived spatial  
715 offset equivalent increased ( $p < 0.0005$ , bootstrap test) with the moving bar luminance (**Fig. 9F**). An even more  
716 interesting psychophysical result is obtained when the moving bar luminance is fixed at a very low detectability  
717 level and the flash luminance is varied. For a sufficiently high flash luminance, the flash-lag effect is reversed  
718 where humans perceive the flash to be in front of the moving bar (flash-lead effect) (Öğmen et al. 2004;  
719 Purushothaman et al. 1998). We again found a qualitatively similar result in our neural data (**Fig. 9G**) where the  
720 perceived spatial offset equivalent decreased ( $p < 0.0005$ , bootstrap test) changing from being positive (flash-  
721 lag) to negative (flash-lead) as the flash luminance level was increased, correlating well with the human  
722 psychophysical results.



723

724

725 **Fig. 9.** Luminance dependence of population response to flash and motion and its correlation to flash lag psychophysics.  
726 **A**, Normalized firing rate responses to flash (dotted trace) and moving bar (solid trace) averaged across multiunits ( $n = 256$ ) from all sessions ( $n = 7$ ) from monkey L. In each subpanel the flash and moving bar had the same luminance  
727 (indicated on the top left corner). **B**, Response peak latencies as a function of luminance, for flash and motion obtained  
728 from the data shown in **A**. Error bars: 95% bootstrap percentile-based plug-in estimate of confidence intervals. **C**,  
729 Luminance dependence of latency difference (flash latency minus motion latency, right vertical axis) computed from data  
730 shown in **B**. Left vertical axis shows perceived spatial offset equivalent computed by multiplying the latency difference  
731 by speed (18 °/s). Error bars as in **B**. **D**, Psychometric functions from human subject MS (for each data point,  $n = 100$   
732 trials, pooled from 5 sessions; for subject SP,  $n = 40$  trials (2 sessions) per data point). The probability of the subject  
733 reporting that the flash is spatially lagging the moving bar is plotted against the veridical spatial offsets between the flash  
734 and moving bar at two luminance values (indicated at the bottom right corner). Error bars as in **B**. **E**, Luminance  
735 dependence of perceived spatial offsets for human subjects (MS and SP). The perceived spatial offsets were computed  
736 from the psychometric functions using the method of compensation. Error bars as in **B**. **F** and **G**, Latency difference and  
737 perceived spatial offset equivalent as a function of moving bar luminance (**F**) for a constant flash luminance ( $0.2 \text{ cd/m}^2$ )  
738 or as a function of flash luminance (**G**) for a constant moving bar luminance ( $0.2 \text{ cd/m}^2$ ). The dotted line in **G** separates the  
739 luminance conditions that gave rise to perceived spatial offset equivalent corresponding to psychophysically measured  
740 flash-lag ('Lag') and flash-lead ('Lead') conditions. Error bars as in **B**.



742

743 **Fig. 10.** Effect of motion direction on perceived spatial offset and its neural equivalent. Illustration of motion directions  
744 (**A**) defined for a given neuron as *foveopetal* if the trajectory hits the receptive field (RF, dotted circles, hypothetical)  
745 before crossing the vertical meridian and *foveofugal* if the trajectory crosses the vertical meridian before hitting the  
746 receptive field. For psychophysics, the same convention applies with the subjects making relative position judgement of  
747 bar stimuli at the RF locations. Speed and moving direction dependence of average perceived spatial offsets in humans (**B**,  
748 n = 8) and monkeys (**D**, n = 2; individual monkey (B and H) data in **C**) computed from data presented in (Subramaniyan et  
749 al. 2013). Speed and moving direction dependence of multiunit response peak latencies (**E**) and the perceived spatial offset  
750 equivalent (**F**) for the individual monkeys (n = 177 (A), 166 (CH) and 180 (CL)) and its average (**G**). Luminance and  
751 motion direction dependence of multiunit response peak latencies (**H**) and the perceived spatial offset equivalent (**I**) in  
752 monkey L (n = 256).

753

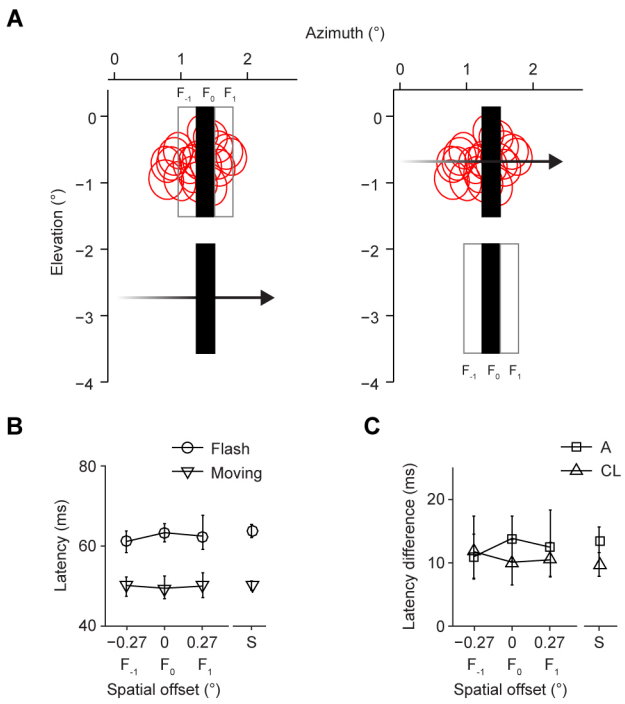
754 **Dependence of latency difference on motion direction**

755 In addition to speed and luminance, the direction of motion has also been shown to affect the perceived spatial  
756 offset. Humans report a larger spatial offset for motion towards fovea (foveopetal, **Fig. 10A**) than motion away  
757 from fovea (foveofugal) (Kanai et al. 2004; Mateeff et al. 1991; Shi and Nijhawan 2008). We reproduced this  
758 finding in our stimulus paradigm where humans reported a higher spatial offset for foveopetal motion direction  
759 in a speed dependent manner (**Fig. 10B**, significant speed effect:  $F(1, 93.2) = 14.8, p < 0.001$ ; nonsignificant  
760 motion condition effect:  $F(1, 75.8) = 2.56, p = 0.11$ ; significant speed x motion condition interaction:  $F(1,$   
761  $79.2) = 10.4, p < 0.01$ ). Surprisingly, in the monkeys this motion effect was reversed under the same stimulus  
762 conditions (**Fig. 10C & D**, significant main effects and interaction: speed:  $F(1, 64) = 27.3, p < 0.001$ ; motion  
763 condition:  $F(1, 67.6) = 12, p = 0.001$ ; speed x motion condition:  $F(1, 64.8) = 6.6, p = 0.013$ ). Correlating with  
764 this, the neural response latencies were lower (**Fig. 10E**) and the perceived spatial offset equivalent were higher  
765 (**Fig. 10F & G**), for the foveofugal condition in two of the three monkeys (latency and perceived spatial offset  
766 equivalent:  $p < 0.0005$  for CH and CL and  $p > 0.05$  for A; Bonferroni corrected for multiple speeds, bootstrap  
767 test). Note that in the neural data from all three monkeys (CH, CL & A), the receptive fields were in the right  
768 hemifield. Consequently, foveopetal condition is inseparable from motion from right to left visual hemifield and  
769 the neural effect we observed may reflect the later rather than the former condition. However, this is less likely  
770 for the following reason. In monkey L where we varied stimulus luminance, the receptive fields were in the  
771 hemifield opposite to that of the above other three monkeys (**Fig. 4D**). This led to the foveopetal condition  
772 being coupled with motion from left to right hemifield. Despite this, we observed the same effect found in the  
773 other data set (CH, CL and A), i.e., the latencies were lower (**Fig. 10H**) the perceived spatial offset equivalents  
774 were higher (**Fig. 10I**,  $p < 0.0005$ , Bonferroni corrected, bootstrap test) for foveofugal condition under all  
775 luminance values tested, suggesting that in monkeys, motion away from fovea produces a larger flash lag effect.  
776 The internal consistency between psychophysical and neural data within the monkey species strongly suggests  
777 that latency difference can explain a species-specific aspect of the flash lag illusion.

778 **Simultaneous presentation of flashed and moving stimuli**

779 In summary, our physiological data from speed and luminance manipulation are in good agreement with  
780 psychophysical results and the predictions of the differential latency model of the flash lag effect. One potential  
781 caveat is that in our physiology experiments we presented the flashes and moving bars in isolation. However, to  
782 generate the flash lag illusion, the flashed and the moving bar are presented simultaneously with perfect  
783 alignment. It is thus conceivable that if we had presented the flash and the moving bar together, the results  
784 might have been different. To rule out this possibility, we conducted a control experiment in which we  
785 presented the flash and moving bar together at different spatial offsets, including a zero-offset condition where  
786 the flashed and the moving bar were in alignment. This allowed us to determine whether there is a change in  
787 latency as a function of spatial offset for simultaneously displayed stimuli.

788 We presented the flashes and moving bars simultaneously ('combined' condition) in two different  
789 arrangements. In the first, we presented flashes at the receptive fields and the moving bar (speed: 14 °/s) outside  
790 the receptive fields (**Fig. 11A**, left panel) and vice versa in the second (**Fig. 11A**, right panel), at 5-7 different  
791 spatial offsets in a gray background. For analysis, we chose the central three offset conditions that had sufficient  
792 number of multiunits (see Methods). We then computed the flash response peak latencies from the first  
793 arrangement and the motion response peak latencies from the second. The latency difference was not  
794 significantly different among the three spatial offsets ( $p > 0.76$ , bootstrap test). In the same recording sessions,  
795 we also presented flashes and moving bars in isolation inside the receptive fields. To test whether in the  
796 combined condition, a second stimulus affected response latencies, we pooled the latency difference data across  
797 monkeys and spatial offsets in the combined condition and compared it to those obtained where stimuli were  
798 presented in isolation ('single' condition; 's' in **Fig. 11B & C**). We found no significant difference between the  
799 combined and the single condition ( $p > 0.99$ , bootstrap test). These results suggest that in awake fixating  
800 macaques, the latencies of the flash or moving bar representation in V1 are not influenced by the presence of a  
801 second bar stimulus outside the classical receptive field.



802

803 **Fig.11.** Control experiment. **A**, Stimulus configurations. The red circles show the outline of receptive fields of a subset of  
 804 the multiunits used in the analysis. Left panel: The filled rectangles show an example stimulus configuration with zero  
 805 spatial offset. The two outlined rectangles show the other locations where we presented the flashes. Right panel: Same as  
 806 the left panel except that the flash is now presented outside the receptive fields. Letter labels ( $F_{-1}$ ,  $F_0$ ,  $F_1$ ) identify flash  
 807 locations whose relative horizontal offsets from moving bar form the abscissa in **B** & **C**. **B**, Response peak latencies of  
 808 flash and moving bar conditions from monkey CL ( $n = 25 \pm 7$  multiunits per condition; mean  $\pm 1$  S.D.; for monkey A,  $n = 14$   
 809  $\pm 3$  per condition), plotted as a function of the horizontal spatial separation between the flash and the instantaneous position  
 810 of the moving bar (spatial offset). Data points from either flash or motion condition presented without an accompanying  
 811 stimulus, are plotted at the abscissa location marked by 'S' ( $n = 76$  multiunits; for monkey A,  $n = 59$ ). Error bars: 95%  
 812 bootstrap percentile-based plug-in estimate of confidence intervals. **C**, Latency difference between flash and moving bar  
 813 conditions from monkey A and CL, plotted as a function of spatial offset. Error bars as in **B**.

#### 814 Population decoding of flashed and moving bars

815 The conclusions reached so far were based on latencies estimated by aligning individual neuronal responses to  
 816 stimulus location in their receptive field centers. However, it is possible that neuronal representation delays  
 817 based on population coding may lead to different conclusions. Hence we proceeded to check if we could  
 818 reproduce the main results of the study presented in **Fig. 7** and **Fig. 9** using probabilistic population decoding  
 819 that does not use any response alignment to receptive field centers to compute representation delays. Rather, the  
 820 moving bar position is decoded based on the population response. Note that this approach was restricted to the  
 821 results presented in **Fig. 7** & **Fig. 9** and not used for results in **Fig. 10** & **Fig.11** because there was an  
 822 insufficient number of neurons for reliable decoding. We also pooled the two motion directions to obtain a  
 823 robust estimate of motion latency especially at high speeds where the moving bar traverses the decoded space  
 824 very quickly giving much fewer trajectory positions to obtain a reliable latency estimate. Similarly, to improve  
 825 the position decoding under the lower luminance conditions where the neural activity is diminished, we  
 826 averaged the motion latencies across the two motion directions.

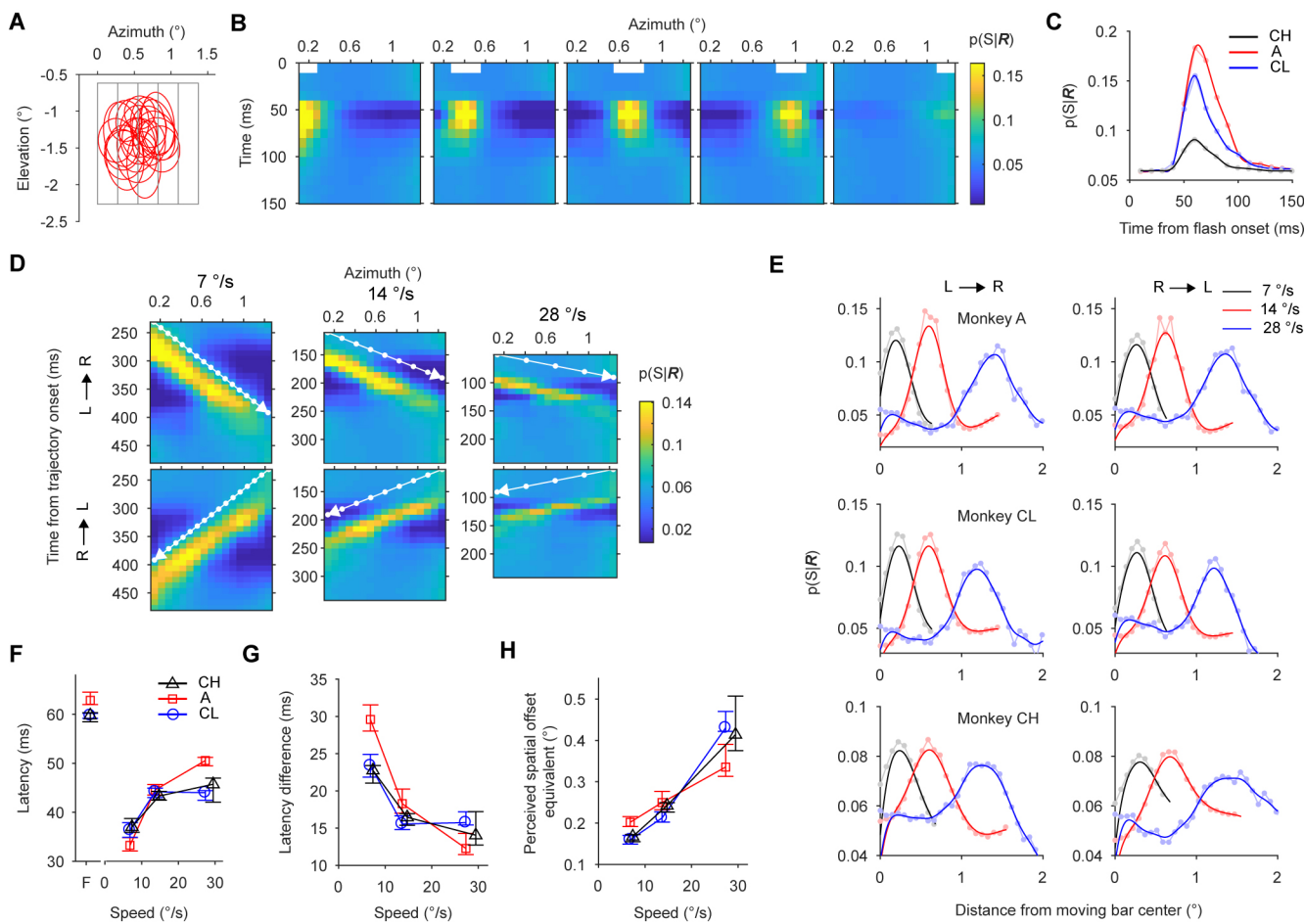
827 A probabilistic Bayesian decoder (see Methods) was used to estimate the representation delays of the stimuli  
 828 based on simultaneously recorded single- or multiunit population activity. We assumed that the neurons spike as  
 829 inhomogeneous Poisson processes that are conditionally independent given the stimulus, and used a decoder  
 830 trained on flashes to decode moving stimuli. It is well-established that population activity in V1 at a given time  
 831 is influenced by the location of the bar stimulus and signal conduction and processing delays. This notion is

832 captured in the forward probabilistic model of population activity in **Fig. 3**. Based on this formalism, a joint  
833 distribution of stimulus location, population activity and response delay was obtained (*Eq. 2*) from which a  
834 posterior probability estimate (*Eq.5*) of a stimulus position can be obtained from the population activity at any  
835 given time. Based on the encoding that was learnt from the flash-evoked responses, we decoded the position of  
836 the moving bar under different speeds and luminance values. For decoding flashes, we used trials that were not  
837 used for encoding to prevent over-fitting. For the luminance modulation experiment, the decoding of bar stimuli  
838 of a given luminance was based on encoding obtained from responses to flashes of matching luminance.

839 The probability of the stimulus position given population activity at different times was computed trial by trial  
840 using simultaneously recorded single-units (**Fig. 13-A**) or multiunits (**Fig. 12-A & Fig. 14-A**) . The resulting  
841 position estimates were first averaged across trials and then across sessions (**Fig. 12-Fig. 14, B & D**). The latency  
842 of the peak of the posterior probability (**Fig. 12-Fig. 14, C**) was taken as the representation delay of the flashes.  
843 For the moving bars, first we computed the distance (spatial lag) between the most probable stimulus location  
844 and the instantaneous location of the moving bar. Towards this, the trial and session-averaged posterior  
845 probabilities (rows in **Fig. 12-Fig. 14 D**) were aligned (centered) to the instantaneous horizontal positions of the  
846 moving bar center (white dots in **Fig. 12-Fig. 14 D**). For each speed and direction, the aligned probabilities were  
847 averaged across the instantaneous positions of the motion trajectory (**Fig. 12-Fig. 14, E**). The distance between  
848 the peak of this aligned probability and the origin gives the spatial lag of the most probable stimulus location.  
849 Note that we did not intend to decode the motion speed hence we treated it as a known quantity. The latency of  
850 the moving bar representation was then computed by dividing the spatial lag by speed.

851 As reported in **Fig. 7B-D**, in all three monkeys, based on multiunit population decoding, as speed increased, the  
852 motion latency increased (**Fig. 12F**,  $p < 0.0005$ , Bootstrap test), latency difference decreased (**Fig. 12G**,  $p <$   
853  $0.0005$ , Bootstrap test), and the perceived spatial offset equivalent increased (**Fig. 12-H**,  $p < 0.0005$ , Bootstrap  
854 test). From one of the monkeys (CL), we were able to isolate a sufficiently large number of single units, so we  
855 were able to verify that the results held true for single well-isolated neurons (**Fig. 13 F-H**) as well.

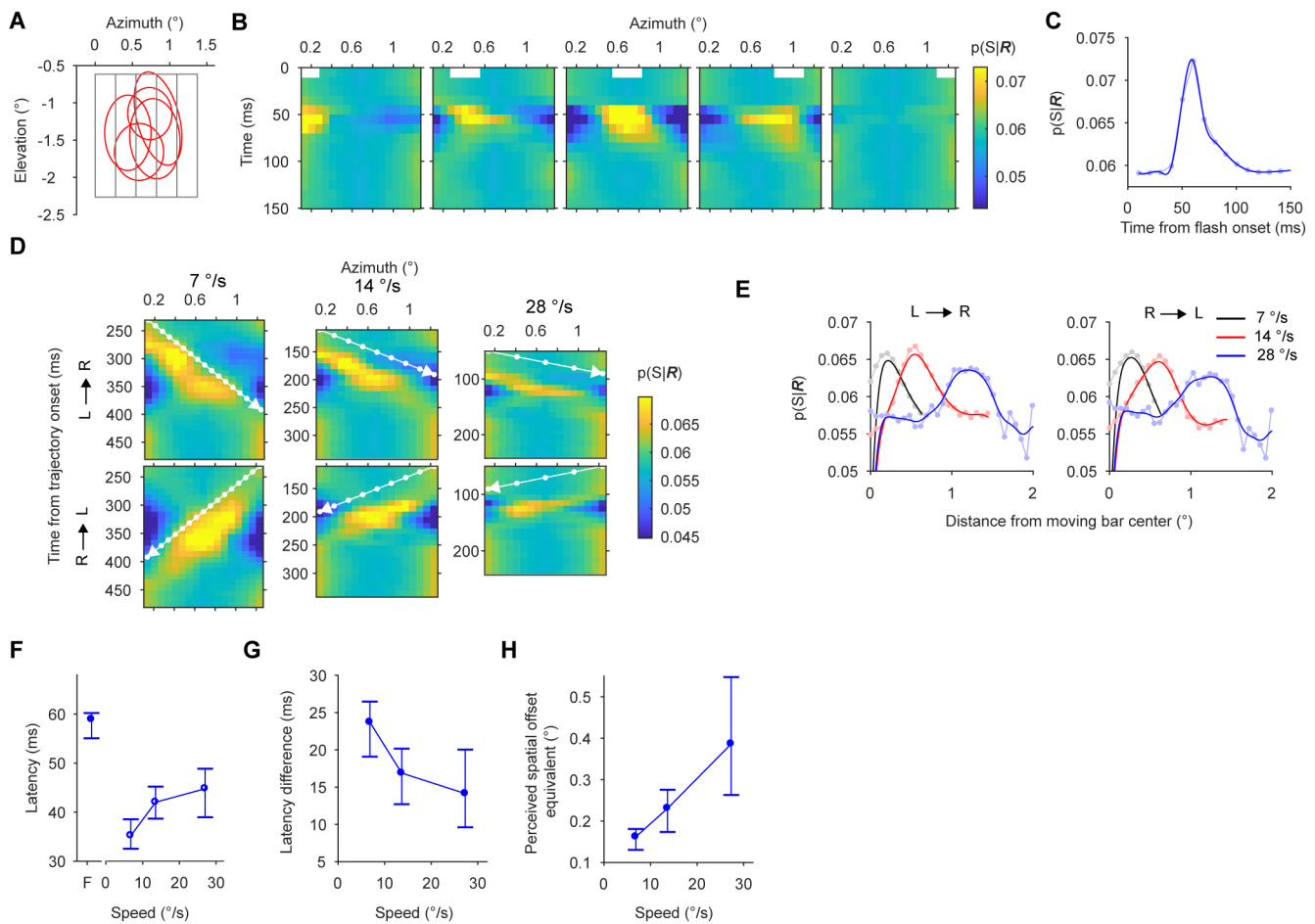
856 For the luminance modulation experiment, we decoded stimulus position for flashes (**Fig. 14B-C**) and moving  
857 bars (**Fig. 14D & E**) as described above. Again, as found before in **Fig. 9**, the multiunit population decoding  
858 showed that for all luminance values tested, the latency of moving bar was less than that of flashes (**Fig. 14 F**,  $p$   
859  $< 0.0005$ , Bonferroni corrected), latency difference and perceived spatial offset equivalent decreased with  
860 luminance (**Fig. 14 G**,  $p < 0.0005$ , Bootstrap test). Similarly, the perceived spatial offset equivalent increased  
861 with moving bar luminance when flash luminance was fixed at the lowest value tested (**Fig. 14 H**,  $p < 0.0005$ ,  
862 Bootstrap test). When the moving bar luminance was fixed at the lowest value tested, the perceived spatial  
863 offset equivalent decreased (**Fig. 14 I**,  $p < 0.0005$ , Bootstrap test) changing from being positive (flash-lag) to  
864 negative (flash-lead) as the flash luminance level was increased. These results suggest that our conclusions on  
865 speed and luminance dependence of latencies and perceived spatial offset equivalents based on individual  
866 multiunit responses are consistent with those obtained by population decoding.



867

868 **Fig. 12.** Population multiunit activity decoding of flashes and moving bars and its relationship to flash lag psychophysics  
 869 under speed manipulation. **A**, Outlines of receptive fields (red) of simultaneously recorded multiunits from a single  
 870 representative session. The gray rectangles show the outlines of different flashes presented one at a time. **B**, Flash  
 871 decoding results from monkey CL: the white box shown near the top of each panel marks the horizontal position of flash in  
 872 space and time. Colors of the plot indicate the average (across trials and sessions) probability ( $p(S|R)$ ) of a horizontal bar  
 873 position (S) given population activity at a given time (R). **C**, Average probability of flash location, pooled across all flash  
 874 conditions for individual monkeys (A, CH and CL). **D**, Average probability of moving bar position for different speeds  
 875 (panel columns) and directions (panel rows, L→R, motion from left to right) for monkey CL. The white arrows indicate  
 876 part of the motion trajectory that lies within the flashed region of space. The white dots on the motion trajectory indicate  
 877 moving bar centers. **E**, Moving bar probability (rows in panel D) aligned to the instantaneous horizontal position (white  
 878 dots in panel D) of the moving bar center. For each speed and direction, the aligned probabilities were averaged across the  
 879 instantaneous positions of the motion trajectory. **F**, Latency of decoding flash and moving bar locations. Flash ('F') latency  
 880 is the latency of peak of flash location probability in panel C. Moving bar latency for a given direction is the product of the  
 881 spatial lag of the peaks of moving bar probabilities in panel E and the inverse of the corresponding speed. Motion latencies  
 882 were then averaged across directions. Error bars: 95% bootstrap percentile-based plug-in estimate of confidence intervals.  
 883 **G**, Speed dependence of the latency difference (Flash minus moving bar latency). Error bars as in F. **H**, Speed dependence  
 884 of perceived spatial offset equivalent obtained by the product of the latency difference and speed. Error bars as in F. Colors  
 885 extremes in B and D are clipped at [0.1, 99.9] percentiles. In C and E, traces of lighter shades with filled circles correspond  
 886 to unsmoothed raw data. Median number of trials (sessions) = 289(9), 604(23), 181(10) and median number of multiunits  
 887 per session (total) = 20(178), 7(166), 19(180) for A, CH and CL respectively.

888

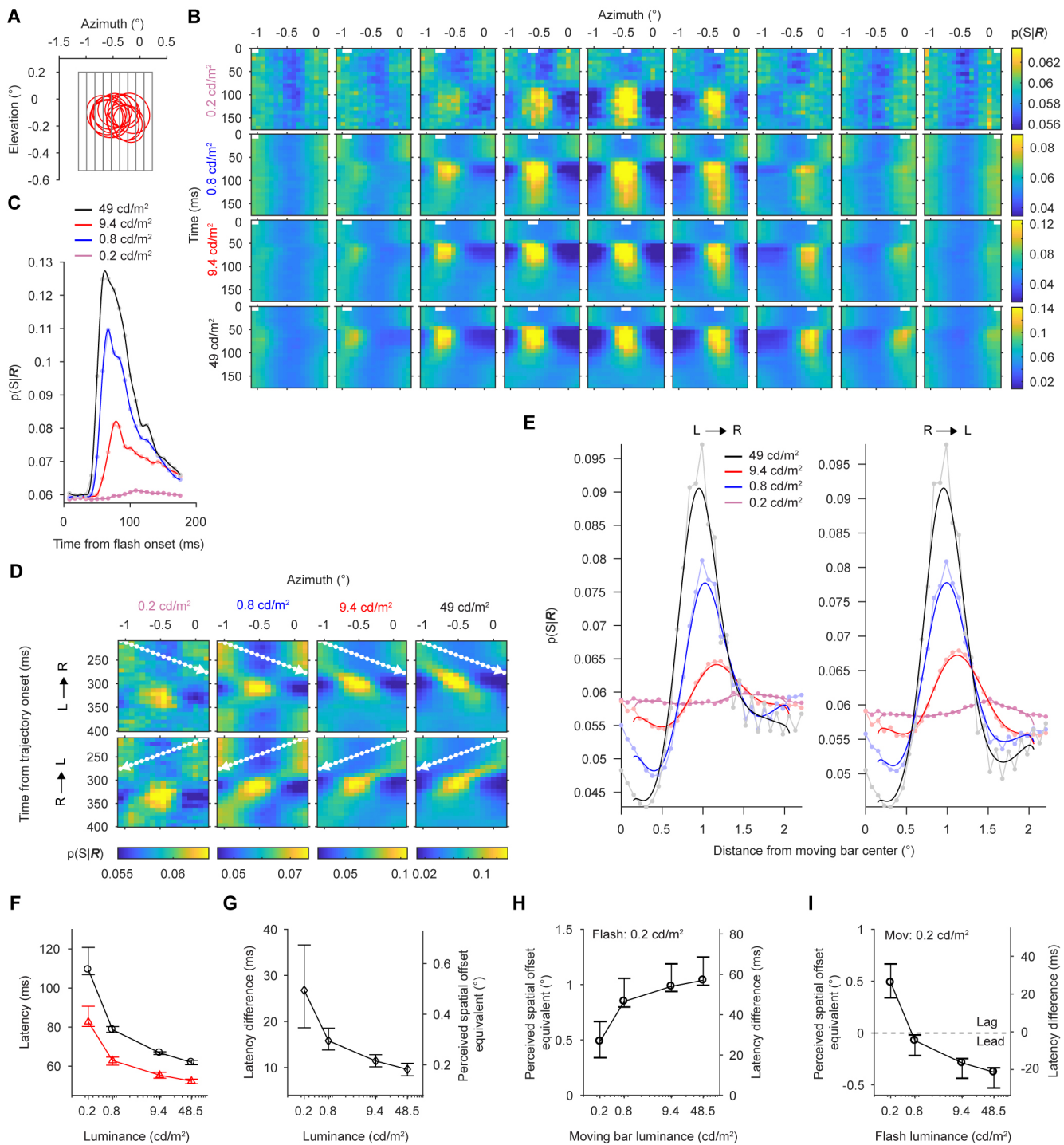


889

**Fig. 13.** Population single-unit activity decoding of flashes and moving bars and its relationship to flash lag psychophysics under speed manipulation. **A**, Outlines of receptive fields (red) of simultaneously recorded single-units from a single representative session. The gray rectangles show the outlines of different flashes presented one at a time. **B**, Flash decoding results from monkey CL: the white box shown near the top of each panel marks the horizontal position of flash in space and time. Colors of the plot indicate the average (across trials and sessions) probability ( $p(S|R)$ ) of a horizontal bar position (S) given population activity at a given time (R). **C**, Average probability of flash location, pooled across all flash conditions for monkey CL. **D**, Average probability of moving bar position for different speeds (panel columns) and directions (panel rows, L  $\rightarrow$  R, motion from left to right) for monkey CL. The white arrows indicate part of the motion trajectory that lies within the flashed region of space. The white dots on the motion trajectory indicate moving bar centers. **E**, Moving bar probability (rows in panel **D**) aligned to the instantaneous horizontal position (white dots in panel **D**) of the moving bar center. For each speed and direction, the aligned probabilities were averaged across the instantaneous positions of the motion trajectory. **F**, Latency of decoding flash and moving bar locations. Flash ('F') latency is the latency of peak of flash location probability in panel **C**. Moving bar latency for a given direction is the product of the spatial lag of the peaks of moving bar probabilities in panel **E** and the inverse of the corresponding speed. Motion latencies were then averaged across directions. Error bars: 95% bootstrap percentile-based plug-in estimate of confidence intervals. **G**, Speed dependence of the latency difference (Flash minus moving bar latency). Error bars as in **F**. **H**, Speed dependence of perceived spatial offset equivalent obtained by the product of the latency difference and speed. Error bars as in **F**. In **B** and **D**, for the set of flash conditions or moving stimuli of a given speed, color boundary was fixed at [0.1, 99.9] percentile. In **C** and **E**, traces of lighter shades with filled circles correspond to unsmoothed raw data. Median number of trials (sessions) = 181(10) and median number of single-units per session (total) = 3(27).

910

911



912

913 **Fig. 14.** Population multiunit activity decoding of flashes and moving bars and its relationship to flash lag psychophysics  
914 under luminance manipulation in monkey L. **A**, Outlines of subset of receptive fields (red) of simultaneously recorded  
915 multiunits from a single representative session. The gray rectangles show the outlines of different flashes presented one at a  
916 time. **B**, Flash decoding results: the white box shown near the top each panel marks the horizontal position of flash in  
917 space and time. The luminance of the bars in each row is indicated on the left. Colors of the plot indicate the average  
918 (across trials and sessions) probability ( $p(S|R)$ ) of a horizontal bar position (S) given population activity at a given time  
919 ( $R$ ). **C**, Average probability of flash location, pooled across all flashes of a given luminance. **D**, Average probability of  
920 moving bar position for different luminance values (panel columns) and directions (panel rows, L→R, motion from left to

921 right). The white arrows indicate part of the motion trajectory (speed, 18 °/s) that lies within the flashed region of space.  
922 The white dots on the motion trajectory indicate moving bar centers. **E**, Moving bar probability (rows in panel **D**) aligned  
923 to the instantaneous horizontal position (white dots in panel **D**) of the moving bar center. For each speed and direction, the  
924 aligned probabilities were averaged across the instantaneous bar positions of the motion trajectory. **F**, Latency of decoding  
925 flash and moving bar locations as a function of luminance. Flash (black trace) latency is the latency of peak of flash  
926 location probability in panel **C**. Moving bar latency (red trace) is the product of the spatial lag of the peaks of moving bar  
927 probabilities in panel **E** and the inverse of the speed. Error bars: 95% bootstrap percentile-based plug-in estimate of  
928 confidence intervals. **G**, Luminance dependence of the latency difference (flash minus moving bar latency, left vertical  
929 axis) and perceived spatial offset equivalent (right vertical axis) obtained by the product of the latency difference and  
930 speed. **H** and **I**, Latency difference and perceived spatial offset equivalent as a function of moving bar luminance (**F**) for a  
931 constant flash luminance (0.2 cd/m<sup>2</sup>) or as a function of flash luminance (**G**) for a constant moving bar luminance (0.2  
932 cd/m<sup>2</sup>). The dotted line in **G** separates the luminance conditions that gave rise to perceived spatial offset equivalent  
933 corresponding to psychophysically measured flash-lag ('Lag') and flash-lead ('Lead') conditions. Error bars as in **B**. In **B**  
934 and **D**, for stimulus conditions under each luminance, color bounds were fixed at [0.1, 99.9] percentile. In **C** and **E**, traces  
935 of lighter shades with filled circles correspond to unsmoothed raw data. Median number of trials (sessions) = 132(7) and  
936 median number of multiunits per session (total) = 39(256).

937

## 938 Discussion

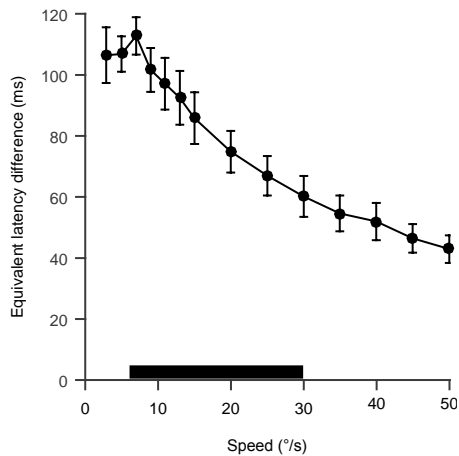
939 Our results show that moving stimuli are processed faster than flashed stimuli in awake macaque V1. In  
940 particular, the latency difference between the neural representations of the two stimuli depends on luminance  
941 and speed in a way that resembles the perceptual effects of these manipulations in both monkeys (Subramaniyan  
942 et al. 2013) and humans (Krekelberg and Lappe 1999; Murakami 2001; Nijhawan 1994; Öğmen et al. 2004;  
943 Patel 2000; Purushothaman et al. 1998; Subramaniyan et al. 2013).

944 Both pre-cortical and cortical mechanisms likely contribute to the observed faster motion processing. These  
945 mechanisms potentially include motion induced dynamic shift in the receptive field location and faster  
946 conduction/processing of motion signals. Our data cannot distinguish between these two possibilities since both  
947 will give rise to a shift in motion response relative to flash response. Motion-induced receptive field shifts have  
948 not been reported in the pre-cortical stages in macaques. If found, it would suggest that the labeled line code is  
949 not static but more dynamic and will depend on properties of the stimuli. However, there is some evidence for  
950 shorter latency of motion signals in the pre-cortical stage - the lateral geniculate nucleus (LGN). In anesthetized  
951 cats, it was found that in the different types of LGN cells, the response peak latency for moving bar was shorter  
952 compared to that of flashed bar (Orban et al. 1985). Future studies are needed to confirm these findings in  
953 monkeys in order to locate the mechanisms underlying the flash lag effect. Cortical processing such as gain  
954 control similar to that described in the retina (Berry et al. 1999) and motion-related feedback signals may  
955 contribute to dynamic shift in the receptive field location towards the motion direction. For example a recent  
956 study (Ni et al. 2014) found that V1 receptive fields in fixating macaques shifted by about 10 % (0.1°) on  
957 average in the direction that accounted for the size-distance illusion. Such receptive field shifts if induced by  
958 motion can readily explain part of the faster motion processing. Another study that addressed a different illusion  
959 called flash-jump illusion also found that V4 neuronal receptive fields shift when the color of one of the bars of  
960 an apparent motion sequence changes abruptly (Sundberg et al. 2006). Given that a color change was necessary  
961 for such a shift, the implications of their study to the neural mechanisms of flash lag illusion remains unclear.

962 Faster cortical motion processing could also be achieved by the spreading of subthreshold activity through  
963 lateral connections from the currently activated cortical region into the region activated in the future. This  
964 spread may facilitate responses by bringing the membrane potential of the target neurons closer to threshold. As  
965 a result, those neurons will reach their peak firing earlier, resulting in shorter motion latency. The influence of  
966 such subthreshold activity has already been reported in cat V1 in the context of line-motion illusion where the  
967 spread of subthreshold activity initiated by one stimulus facilitates the response to a subsequently presented  
968 stimulus (Jancke et al. 2004a). Based on this mechanism, it could also be expected that the slower motion would

969 exhibit shorter latency through this mechanism compared to the faster one as there would be more time for the  
970 subthreshold activity to spread farther for the slower compared to the faster motion, potentially explaining the  
971 speed dependence of motion latency we observed.

972 We found that the moving bar response peak latency increased with speed. Consistent with our results,  
973 conversion of the direction-averaged spatial lag data reported by Jancke et al. (2004) (Fig. 6 in their study) into  
974 latency also revealed a similar trend in the speed dependency of motion peak latency. Our data show that  
975 latency difference between flash and motion condition decreased with speed. This is in sharp contrast to the  
976 constant latency difference that most psychophysical studies assume when interpreting the effect of speed in  
977 perceived spatial offset (Krekelberg and Lappe 1999; Murakami 2001; Nijhawan 1994; Whitney et al. 2000).  
978 Equivalent latency difference computed from the perceived spatial offsets from a recent psychophysical study  
979 (Wojtach et al. 2008) however clearly decreases with speed (Fig. 15) similar to our findings. The discrepancy  
980 among the psychophysical studies can be reconciled by noting that Wojtach et al. (2008) used a wide range of  
981 speeds (up to 50 °/s) whereas the previous ones used a narrow speed range (up to ~15 °/s), which missed the full  
982 trend of the speed effect.



983

984 **Fig. 15.** Equivalent latency difference as a function motion speed in humans. The equivalent latency difference (flash  
985 temporally lagging the moving object) data points in the plot were computed by dividing the perceived spatial offset by  
986 speed reported in Fig. 4 of Wojtach et al. (2008). Error bars are  $\pm 1$  SEM. The black bar shows the range of speeds used in  
987 our physiological experiments.

988 We found that the perceived spatial offset equivalent depended on speed and luminance (Fig. 7D, Fig. 9C, Fig.  
989 12-Fig. 13, H and Fig. 14G) in line with psychophysical results (Fig. 7E and Fig. 9E). The magnitude of the  
990 perceived offset computed from the population decoding method appeared to be closer to the behaviorally  
991 measured values than the values computed based on individual multi-unit activity. Interpreting our data  
992 conservatively, we think that the perceived spatial offset equivalents we measured in V1 are likely to be smaller  
993 than the behaviorally measured values for the following reasons. 1) We measured neural responses from the  
994 very first cortical processing stage and the physiological effect may get larger as the information is processed  
995 further in the higher cortical areas, 2) the smaller receptive field sizes in V1 may potentially limit the extent to  
996 which receptive field shifts can occur in order to reduce motion stimulus representation delays and 3) the  
997 monkeys we recorded from did not perform the task and making a relative position judgment may lead to a  
998 larger physiological effect. Moreover, we may have also underestimated the discrepancy between the  
999 behaviorally measured perceived spatial offset and its neural equivalent because we presented flashes randomly  
1000 in multiple locations (5-7) for physiology whereas for psychophysics the flash was presented at one (Fig. 9E) or  
1001 two (Fig. 7E, Fig. 10B-D) fixed locations. Given that predictability of flashes is known to reduce the flash lag  
1002 effect (Baldo et al. 2002; Brenner and Smeets 2000; Krekelberg et al. 2000; Vreven and Verghese 2005), it is  
1003 possible that psychophysical measurement of the lag could have been higher if the flashes were equally  
1004 unpredictable as in our physiology experiments.

1005 It should be noted that the human psychophysical data were collected from two non-naïve subjects whose bias  
1006 could have an effect on the observed data. We think that this is less likely because our results build upon  
1007 previously well-established psychophysical results on luminance manipulation (Lappe and Krekelberg 1998;  
1008 Öğmen et al. 2004; Purushothaman et al. 1998) and are well in accordance with what would be predicted from  
1009 them. Never the less, further experiments from naïve subjects would be essential to confirm our human  
1010 psychophysical results.

1011 In our luminance manipulation experiment, we kept the background luminance near zero and changed only the  
1012 bar luminance. This stimulus configuration, although suitable for mimicking flash lag psychophysical  
1013 experiment, is not readily comparable to previous physiological studies in V1 that examined luminance or  
1014 contrast effect on latency using different stimulus configurations (Carandini and Heeger 1994; Gawne et al.  
1015 1996; Maunsell and Gibson 1992; Oram 2010; Reich et al. 2001). Despite these stimulus differences, similar to  
1016 the above studies, we also observed consistent increase in latency when the flash luminance was lowered. The  
1017 latency for moving bar also increased when the bar luminance was decreased. However, unexpectedly we found  
1018 that luminance manipulation affected the latency of flash and moving bars differently. The latency profile of the  
1019 moving bar response was not simply a downward-shifted version of the flash response latency profile. Instead,  
1020 the increase in latency of moving bar was much less pronounced compared to that of the flash when the  
1021 luminance was low. With the caveat that we examined the luminance effect only in a single monkey, these  
1022 results suggest that moving bars do not suffer as much processing delay as the flashed objects under low  
1023 luminance conditions and likely invoke different set of mechanisms in bringing out the observed latency effect.

1024 Although several aspects of the flash lag illusion were similar between the monkeys and humans, it was  
1025 surprising to find that monkeys reported a larger lag for foveofugal motion as opposed to foveopetal motion as  
1026 found in humans (Kanai et al. 2004; Mateeff et al. 1991; Shi and Nijhawan 2008) and this behavioral effect had  
1027 a neural correlate in three out of four monkeys. Although species difference could be partly responsible for this,  
1028 further investigations are needed to fully understand the sources of the discrepancy.

1029 Our data provide two independent lines of evidence supporting the differential latency (DL) model (Öğmen et  
1030 al. 2004; Patel 2000; Purushothaman et al. 1998; Whitney and Murakami 1998), which predicts shorter time  
1031 needed for representing moving stimuli. First, as predicted, the perceived spatial offset equivalent computed  
1032 directly from the latency difference, increased with the speed of the moving bar. Second, the luminance  
1033 dependence of the flash and motion representation delays (**Fig. 9B**) is also consistent with the key predictions of  
1034 DL (Öğmen et al. 2004; Patel 2000; Purushothaman et al. 1998) namely, for a fixed low flash luminance, the  
1035 perceived spatial offset should increase with moving bar luminance and for a fixed low moving stimulus  
1036 luminance, progressively increasing the flash luminance should change the flash-lag to flash-lead effect. Our  
1037 neural data support both predictions (**Fig. 9F & G**). In addition, latency differences (**Fig. 9C**) also explained the  
1038 trend in the luminance modulation of perceived spatial offset using identical luminance for flash and moving  
1039 bar which we showed in humans (**Fig. 9E**) for the first time.

1040 According to the motion-biasing model (Eagleman and Sejnowski 2007; Rao et al. 2001), the latencies of flash  
1041 and moving bar representations are equal, in contrast to what we find in our data. In addition, the illusion arises  
1042 because “when the brain is triggered to make an instantaneous position judgment, motion signals that stream in  
1043 over ~80 ms after the triggering event (e.g., a flash) will bias the localization” (Eagleman and Sejnowski 2007).  
1044 It is unclear exactly in which parts of the brain this ‘biasing’ process is implemented. Also unclear is whether  
1045 and exactly when V1 spatial representations are altered by this ‘biasing’. Moreover, this model would predict  
1046 that a neural correlate of the motion-biasing would be observed only when the subjects are asked to make an  
1047 explicit relative position judgment to decide if the moving and flashed stimuli are misaligned. However, in our  
1048 main experiments, only a flash or a moving bar was presented in isolation and the animals used in our study  
1049 were neither trained to make any relative position judgment nor were trained in any other task like the current  
1050 task; we still found a neural correlate of the illusion in V1. First, these results suggest that reporting relative  
1051 position judgment is not necessary for observing a neural correlate of the flash lag illusion in visual area V1.  
1052 Second, they argue against the current version of the motion-biasing model that involves only higher cognitive

1053 functions (Eagleman and Sejnowski 2007) and suggest that low level mechanisms underlying the observed  
1054 latency differences need to be taken into account.

1055 While there is substantial evidence against the spatial extrapolation model at the psychophysical level (Baldo  
1056 and Klein 1995; Brenner and Smeets 2000; Eagleman and Sejnowski 2000; Lappe and Krekelberg 1998;  
1057 Purushothaman et al. 1998; Whitney and Murakami 1998), it is possible that spatial extrapolation could be  
1058 happening at the level of V1. Given that any spatial extrapolation would manifest as a reduction in latency as  
1059 measured by our method, a full delay compensation as predicted by the model would result in zero response  
1060 peak latency for the moving bar. However, this was not the case as we found significant delays for the moving  
1061 bar at all speed and luminance conditions tested. Nevertheless, spatial extrapolation might still hold true in other  
1062 brain regions or for other sensory systems as shown for auditory motion (Witten et al. 2006).

1063 Irrespective of the model of the flash lag illusion, if the motion representation/perception delays are not  
1064 ultimately reduced to zero, moving objects will always be mislocalized. Our results suggest that the overall  
1065 shorter motion latency compared to flashes helps to reduce this mislocalization. Given our results that motion  
1066 response latencies also change with speed and luminance, how would organisms cope with this in behaviors that  
1067 require accurate localization of moving objects? One simple and viable solution would be calibration of the  
1068 sensorimotor integration system. For example, to accurately hit the ball in baseball game, players spend  
1069 numerous hours in learning (calibrating) to swing the bat at the correct time taking the speed of the ball into  
1070 account. Hence, the nervous system could in principle learn to respond appropriately to a given moving  
1071 stimulus condition.

1072 We focused our study on V1 where both flash and motion signals first arrive in the cortex. We showed that  
1073 moving objects are processed faster in a speed, direction of motion and luminance dependent way compared to  
1074 suddenly appearing static stimuli. These provide a neural correlate of the flash lag illusion. In this visual area,  
1075 our data are fully consistent with the predictions of the differential latency model. While the motion-biasing  
1076 model cannot explain our results, this in itself is not evidence against the model in its entirety. It is possible that  
1077 the monkeys need to perform the task for the mechanisms proposed by the model to be activated. Visual signals  
1078 leaving V1 reach a multitude of cortical areas. It is yet to be seen if the differential latency theory would hold in  
1079 these other areas. Hence further combined behavioral and physiological studies in V1 and subsequent  
1080 processing stages in the brain are essential to generate additional constraints to narrow down the models.

1081  
1082 *Acknowledgements:* This work was supported by the National Eye Institute-United States National Institutes of  
1083 Health (NIH) Grants R01 EY018847, 5-T32-EY07001-37, 5-P30- EY002520-33, the Bernstein Center for  
1084 Computational Neuroscience (FKZ 01GQ1002), the German Excellency Initiative through the Centre for  
1085 Integrative Neuroscience Tübingen (EXC307), the Bernstein Award for Computational Neuroscience to  
1086 PB (BMBF, FKZ 01GQ1601), a Heisenberg Professorship to PB (DFG 5601/4-1) and a German Research  
1087 Foundation (DFG) grant to ASE (DFG EC 479/1-1). We thank D. Murray, T. Shinn and A. Laudano for  
1088 technical assistance.

1089  
1090  
1091 *Conflict of Interest:* The authors declare no competing financial interests.  
1092

1093

1094

1095

1096 **References**

1097 **Bachmann T, and Poder E.** Change in feature space is not necessary for the flash-lag effect. *Vision Res* 41:  
1098 1103-1106, 2001.

1099 **Baldo MV, Kihara AH, Namba J, and Klein SA.** Evidence for an attentional component of the perceptual  
1100 misalignment between moving and flashing stimuli. *Perception* 31: 17-30, 2002.

1101 **Baldo MV, and Klein SA.** Extrapolation or attention shift? *Nature* 378: 565-566, 1995.

1102 **Berry MJ, 2nd, Brivanlou IH, Jordan TA, and Meister M.** Anticipation of moving stimuli by the retina.  
1103 *Nature* 398: 334-338, 1999.

1104 **Brainard DH.** The Psychophysics Toolbox. *Spat Vis* 10: 433-436, 1997.

1105 **Brenner E, and Smeets JB.** Motion extrapolation is not responsible for the flash-lag effect. *Vision Res* 40:  
1106 1645-1648, 2000.

1107 **Carandini M, and Heeger DJ.** Summation and division by neurons in primate visual cortex. *Science* 264:  
1108 1333-1336, 1994.

1109 **Dayan P, and Abbott LF.** *Theoretical Neuroscience: Computational and Mathematical Modeling of Neural*  
1110 *Systems*. The MIT Press, 2005.

1111 **Eagleman DM, and Sejnowski TJ.** Motion integration and postdiction in visual awareness. *Science* 287: 2036-  
1112 2038, 2000.

1113 **Eagleman DM, and Sejnowski TJ.** Motion signals bias localization judgments: A unified explanation for the  
1114 flash-lag, flash-drag, flash-jump, and Frohlich illusions. *J Vis* 7: 3-3, 2007.

1115 **Ecker AS, Berens P, Cotton RJ, Subramaniyan M, Denfield GH, Cadwell CR, Smirnakis SM, Bethge M,**  
1116 **and Tolias AS.** State dependence of noise correlations in macaque primary visual cortex. *Neuron* 82: 235-248,  
1117 2014.

1118 **Ecker AS, Berens P, Keliris GA, Bethge M, Logothetis NK, and Tolias AS.** Decorrelated Neuronal Firing in  
1119 Cortical Microcircuits. *Science* 327: 584-587, 2010.

1120 **Efron B, and Tibshirani RJ.** *An Introduction to the Bootstrap*. Taylor & Francis, 1994.

1121 **Frund I, Haenel NV, and Wichmann FA.** Inference for psychometric functions in the presence of  
1122 nonstationary behavior. *J Vis* 11: 1-19, 2011.

1123 **Gawne TJ, Kjaer TW, and Richmond BJ.** Latency: another potential code for feature binding in striate  
1124 cortex. *J Neurophysiol* 76: 1356-1360, 1996.

1125 **Jancke D, Chavane F, Naaman S, and Grinvald A.** Imaging cortical correlates of illusion in early visual  
1126 cortex. *Nature* 428: 423-426, 2004a.

1127 **Jancke D, Erlhagen W, Schoner G, and Dinse HR.** Shorter latencies for motion trajectories than for flashes  
1128 in population responses of cat primary visual cortex. *J Physiol* 556: 971-982, 2004b.

1129 **Kanai R, Sheth BR, and Shimojo S.** Stopping the motion and sleuthing the flash-lag effect: spatial uncertainty  
1130 is the key to perceptual mislocalization. *Vision Res* 44: 2605-2619, 2004.

1131 **Khoei MA, Masson GS, and Perrinet LU.** The Flash-Lag Effect as a Motion-Based Predictive Shift. *PLoS*  
1132 *Comput Biol* 13: e1005068, 2017.

1133 **Kleiner M, Brainard, D and Pelli, D.** What's new in Psychtoolbox-3? *Perception* 36: 2007.

1134 **Krekelberg B, and Lappe M.** A model of the perceived relative positions of moving objects based upon a slow  
1135 averaging process. *Vision Res* 40: 201-215, 2000.

1136 **Krekelberg B, and Lappe M.** Temporal recruitment along the trajectory of moving objects and the perception  
1137 of position. *Vision Res* 39: 2669-2679, 1999.

1138 **Krekelberg B, Lappe M, Whitney D, Cavanagh P, Eagleman DM, and Sejnowski TJ.** The position of  
1139 moving objects. *Science* 289: 1107a, 2000.

1140 **Lappe M, and Krekelberg B.** The position of moving objects. *Perception* 27: 1437-1449, 1998.

1141 **Ma WJ, Beck JM, Latham PE, and Pouget A.** Bayesian inference with probabilistic population codes. *Nat*  
1142 *Neurosci* 9: 1432-1438, 2006.

1143 **Mackay DM.** Perceptual stability of a stroboscopically lit visual field containing self-luminous objects. *Nature*  
1144 181: 507-508, 1958.

1145 **Mateeff S, Yakimoff N, Hohnsbein J, Ehrenstein WH, Bohdanecky Z, and Radil T.** Selective directional  
1146 sensitivity in visual motion perception. *Vision Res* 31: 131-138, 1991.

1147 **Maunsell JH, and Gibson JR.** Visual response latencies in striate cortex of the macaque monkey. *J*  
1148 *Neurophysiol* 68: 1332-1344, 1992.

1149 **Murakami I.** The flash-lag effect as a spatiotemporal correlation structure. *J Vis* 1: 126-136, 2001.

1150 **Ni AM, Murray SO, and Horwitz GD.** Object-centered shifts of receptive field positions in monkey primary  
1151 visual cortex. *Curr Biol* 24: 1653-1658, 2014.

1152 **Nijhawan R.** Motion extrapolation in catching. *Nature* 370: 256-257, 1994.

1153 **Öğmen H, Patel SS, Bedell HE, and Camuz K.** Differential latencies and the dynamics of the position  
1154 computation process for moving targets, assessed with the flash-lag effect. *Vision Res* 44: 2109-2128, 2004.

1155 **Oram MW.** Contrast induced changes in response latency depend on stimulus specificity. *J Physiol Paris* 104:  
1156 167-175, 2010.

1157 **Orban GA, Hoffmann KP, and Duysens J.** Velocity selectivity in the cat visual system. I. Responses of LGN  
1158 cells to moving bar stimuli: a comparison with cortical areas 17 and 18. *J Neurophysiol* 54: 1026-1049, 1985.

1159 **Patel SS.** Flash-Lag Effect: Differential Latency, Not Postdiction. *Science* 290: 1051a-1051, 2000.

1160 **Pelli DG.** The VideoToolbox software for visual psychophysics: transforming numbers into movies. *Spat Vis*  
1161 10: 437-442, 1997.

1162 **Purushothaman G, Patel SS, Bedell HE, and Ogom H.** Moving ahead through differential visual latency.  
1163 *Nature* 396: 424, 1998.

1164 **Rao RP, Eagleman DM, and Sejnowski TJ.** Optimal smoothing in visual motion perception. *Neural Comput*  
1165 13: 1243-1253, 2001.

1166 **Reich DS, Mechler F, and Victor JD.** Temporal coding of contrast in primary visual cortex: when, what, and  
1167 why. *J Neurophysiol* 85: 1039-1050, 2001.

1168 **Sanger TD.** Probability density estimation for the interpretation of neural population codes. *J Neurophysiol* 76:  
1169 2790-2793, 1996.

1170 **Sheth BR, Nijhawan R, and Shimojo S.** Changing objects lead briefly flashed ones. *Nat Neurosci* 3: 489-495,  
1171 2000.

1172 **Shi Z, and Nijhawan R.** Behavioral significance of motion direction causes anisotropic flash-lag, flash-drag,  
1173 flash-repulsion, and movement-mislocalization effects. *J Vis* 8: 24 21-14, 2008.

1174 **Subramanyan M, Ecker AS, Berens P, and Tolias AS.** Macaque monkeys perceive the flash lag illusion.  
1175 *PLoS ONE* 8: e58788, 2013.

1176 **Sundberg KA, Fallah M, and Reynolds JH.** A Motion-Dependent Distortion of Retinotopy in Area V4.  
1177 *Neuron* 49: 447-457, 2006.

1178 **Tolias AS, Ecker AS, Siapas AG, Hoenselaar A, Keliris GA, and Logothetis NK.** Recording Chronically  
1179 From the Same Neurons in Awake, Behaving Primates. *J Neurophysiol* 98: 3780-3790, 2007.

1180 **Vreven D, and Verghese P.** Predictability and the dynamics of position processing in the flash-lag effect.  
1181 *Perception* 34: 31-44, 2005.

1182 **Whitney D, and Murakami I.** Latency difference, not spatial extrapolation. *Nat Neurosci* 1: 656-657, 1998.

1183 **Whitney D, Murakami I, and Cavanagh P.** Illusory spatial offset of a flash relative to a moving stimulus is  
1184 caused by differential latencies for moving and flashed stimuli. *Vision Res* 40: 137-149, 2000.

1185 **Wichmann FA, and Hill NJ.** The psychometric function: I. Fitting, sampling, and goodness of fit. *Percept  
1186 Psychophys* 63: 1293-1313, 2001a.

1187 **Wichmann FA, and Hill NJ.** The psychometric function: II. Bootstrap-based confidence intervals and  
1188 sampling. *Percept Psychophys* 63: 1314-1329, 2001b.

1189 **Witten IB, Bergan JF, and Knudsen EI.** Dynamic shifts in the owl's auditory space map predict moving  
1190 sound location. *Nat Neurosci* 9: 1439-1445, 2006.

1191 **Wojtach WT, Sung K, Truong S, and Purves D.** An empirical explanation of the flash-lag effect.  
1192 *Proceedings of the National Academy of Sciences* 105: 16338-16343, 2008.

1193 **Zhang K, Ginzburg I, McNaughton BL, and Sejnowski TJ.** Interpreting neuronal population activity by  
1194 reconstruction: unified framework with application to hippocampal place cells. *J Neurophysiol* 79: 1017-1044,  
1195 1998.

1196